AEDC-TN-60-219

(TITLE UNCLASSIFIED)

INVESTIGATION OF STATIC STABILITY AND AERODYNAMIC EFFECTS OF CONTROL JETS ON A 1/3-SCALE PYE WACKET MISSILE AT TRANSONIC MACH NUMBERS

By

D. C. Baker and L. L. Galigher
PWT, ARO, Inc.

December 1960

ARNOLD ENGINEERING DEVELOPMENT CENTER

AIR RESEARCH AND DEVELOPMENT COMMAND

U S A F

[redacted]

(Title Unclassified)

INVESTIGATION OF STATIC STABILITY AND AERODYNAMIC EFFECTS OF CONTROL JETS ON A 1/3-SCALE PYE WACKET MISSILE AT TRANSONIC MACH NUMBERS

CLASSIFICATION CANCELLED (CHANGED TO [redacted]
BY AUTHORITY OF Det #4, WADD, Eglin AFB Fla., Ltr. of Feb 15, '61 (WWTAW)
BY T. CATHEY 2/20/61
Name and Position of Individual Date

By

D. C. Baker and L. L. Galigher
PWT, ARO, Inc.

This document has been approved for public release and sale; its distribution is unlimited.

[redacted] DOCUMENT

"This material contains information affecting the national defense of the United States within the meaning of the Espionage Laws, Title 18, U.S.C., Sections 793 and 794, the transmission or revelation of which in any manner to an unauthorized person is prohibited by law."

CLASSIFICATION CANCELLED (~~CHANGED TO~~ ....)
BY AUTHORITY OF
Official authorized to change
BY
Name and Position of Individual Date

December 1960
ARO Project No. 221048
Contract No. AF 40(600)-800 S/A 11(60-110)

[redacted]

DECLASSIFIED - UNCLASSIFIED

ABSTRACT

Wind tunnel tests were conducted in the 16-Foot Transonic Circuit, Propulsion Wind Tunnel (PWT), on a lenticular shaped 1/3-scale model of the Pye Wacket missile. The static stability characteristics and the effect of control jets on model pressure distributions were determined at Mach numbers from 0.6 to 1.6, angles of attack from 0 to 9 deg, and yaw angles from 0 to 180 deg. The Reynolds number per foot varied from 1.30 to 3.75 million.

Large changes in force and moment characteristics occurred for extreme yaw angles at subsonic speeds. The control jets produced large aerodynamic interactions at supersonic speeds which increased the control effectiveness of the jets.

CONTENTS

	Page
ABSTRACT	2
NOMENCLATURE	6
INTRODUCTION	8
APPARATUS	
Test Facility	8
Test Article	8
Instrumentation	9
TEST DESCRIPTION	
Test Procedure and Conditions	9
Corrections	11
Precision of Measurements	11
RESULTS AND DISCUSSION	
Force Characteristics	12
Jet Effects	14
CONCLUSIONS	16
REFERENCES	17

TABLE

1. Precision of Measurements	17

ILLUSTRATIONS

Figure		
1.	Model Installation and Details of the Perforated Walls	18
2.	Pye Wacket Model Installation in the PWT	19
3.	Model Dimensions	20
4.	Model Axis System	21
5.	Pressure Orifice Locations	22
6.	View of the Instrumented Side of the Model Mounted at the 180-deg Yaw Position	23
7.	Test Conditions for the Pye Wacket Model	
	a. Dynamic Pressure	24
	b. Reynolds Number Per Foot	24

Figure		Page
8.	Variation of Normal-Force Coefficient with Angle of Attack, ψ = 0 and 90	25
9.	Variation of Normal-Force Coefficient with Angle of Attack, ψ = 180	26
10.	Model Centerline Pressure Coefficient Distribution, M_∞ = 0.8, α = 3.2	27
11.	Model Centerline Pressure Coefficient Distribution, M_∞ = 1.0, α = 3.2	28
12.	Effect of Angle of Attack and Mach Number on Pitching-Moment Coefficient, ψ = 0 and 90	29
13.	Effect of Angle of Attack and Mach Number on Pitching-Moment Coefficient, ψ = 180	30
14.	Variation of Normal-Force Curve Slope with Mach Number, ψ = 0	31
15.	Variation of Pitching-Moment Curve Slope with Mach Number, ψ = 0	31
16.	Effect of Angle of Attack and Angle of Yaw on Center of Pressure Location	32
17.	Effect of Yaw Angle on Center of Pressure Location, M_∞ = 0.8 and 1.0, α = 6.4	33
18.	Variation of Side-Force Coefficient with Yaw Angle, α = 0	34
19.	Variation of Side-Force Coefficient with Yaw Angle, M_∞ = 0.8	35
20.	Variation of Side-Force Coefficient with Yaw Angle, M_∞ = 1.0	36
21.	Variation of Yawing-Moment Coefficient with Yaw Angle, α = 0	37
22.	Variation of Yawing-Moment Coefficient with Yaw Angle, M_∞ = 0.8	38
23.	Variation of Yawing-Moment Coefficient with Yaw Angle, M_∞ = 1.0	39

Figure		Page
24.	Variation of Rolling-Moment Coefficient with Yaw Angle, $M_\infty = 0.8$	40
25.	Variation of Rolling-Moment Coefficient with Yaw Angle, $M_\infty = 1.0$	41
26.	Variation of Forebody and Base-Drag Coefficient with Mach Number, $\alpha = 0$, $\psi = 0$	42
27.	Effect of Jet Flow on Normal-Force Coefficient, $\psi = 0$	
	a. Upper Surface Jets-On	43
	b. Lower Surface Jets-On	43
28.	Effect of Jet Flow on Pitching-Moment Coefficient, $\psi = 0$	
	a. Upper Surface Jets-On	44
	b. Lower Surface Jets-On	44
29.	Effect of Upper Surface Jet Flow on Normal-Force Coefficient, $\alpha = 0$	45
30.	Effect of Upper Surface Jet Flow on Pitching-Moment Coefficient, $\alpha = 0$	46
31.	Effect of Jet Exit Pressure Ratio on Normal-Force and Pitching-Moment Coefficient with Upper Surface Jets On, $M_\infty = 1.2$, $\alpha = 0$, $\psi = 0$	47
32.	Influence of Control Jet Flow on Pressure Coefficient Distribution about the Jet Exit, $M_\infty = 0.6$, $\alpha = 0$, $\psi = 0$	48
33.	Influence of Control Jet Flow on Pressure Coefficient Distribution about the Jet Exit, $M_\infty = 1.4$, $\alpha = 0$, $\psi = 0$	49

NOMENCLATURE

A_b	Model base area, 0.41736 ft²
C_A	Axial-force coefficient, axial force/q_∞ S
$C_{A,b}$	Base axial-force coefficient, $(p_\infty - p_b)A_b/q_\infty$ S
$C_{A,F}$	Forebody axial-force coefficient, $C_A - C_{A,b}$
C_l	Rolling-moment coefficient, rolling moment/q_∞ SD
C_m	Pitching-moment coefficient, pitching moment/q_∞ SD
C_{mj}	Equivalent pitching-moment coefficient due to the jet thrust, positive in the direction of the positive pitching moment, jet pitching moment/q_∞ SD
C_{m_α}	Rate of change of pitching-moment coefficient with angle of attack, $dC_m/d\alpha$, evaluated at $C_m = 0$, per deg
C_N	Normal-force coefficient, normal force/q_∞ S
C_{Nj}	Equivalent normal-force coefficient due to the jet thrust, positive in the direction of the positive normal-force coefficient, jet thrust/q_∞ S
C_{N_α}	Rate of change of normal-force coefficient with angle of attack, $dC_N/d\alpha$, evaluated at $C_N = 0$, per deg
C_n	Yawing-moment coefficient, yawing moment/q_∞ SD
C_p	Pressure coefficient, $(p_l - p_\infty)/q_\infty$
C_Y	Side-force coefficient, side force/q_∞ S
ΔC_m	Change in pitching-moment coefficient $(C_{m_{\text{jets on}}} - C_{m_{\text{jets off}}})$ calculated by numerical integration of the model surface pressures
ΔC_N	Change in normal-force coefficient $(C_{N_{\text{jets on}}} - C_{N_{\text{jets off}}})$ calculated by numerical integration of the model surface pressures
D	Model diameter, 1.667 ft
M_∞	Free-stream Mach number

p_b	Static pressure on model base, lb/ft^2
p_e	Jet exit static pressure, lb/ft^2
p_l	Local static pressure, lb/ft^2
p_∞	Free-stream static pressure, lb/ft^2
q_∞	Free-stream dynamic pressure, $0.7\ p_\infty M_\infty^2$, lb/ft^2
R	Reynolds number per foot, V_∞/ν_∞
r_1	Distance from center of jet to the first radial ring of orifices around the jet, 0.475 in.
r_2	Distance from center of jet to the second radial ring of orifices around the jet, 1.35 in.
r_3	Distance from center of jet to the third radial ring of orifices around the jet, 2.225 in.
S	Model planform area, 2.1817 ft^2
V_∞	Free-stream velocity, ft/sec
x	Distance from the center of the model, positive along the positive x-axis, ft
x_{cp}	Center of pressure location expressed in body diameters from the center of the model, positive along the positive x-axis, C_m/C_N
y_{cp}	Center of pressure location expressed in body diameters from the center of the model, positive along the positive y-axis, C_l/C_N
α	Angle of attack, positive nose up, deg
ν_∞	Kinematic viscosity of the free-stream, ft^2/sec
ψ	Angle of yaw, deg
ψ_b	Model attachment positions, 0, 90, 180 deg

INTRODUCTION

At the request of the Air Proving Ground Center, Eglin Air Force Base, Florida, tests of a 1/3-scale Pye Wacket missile were conducted in the PWT 16-Foot Transonic Circuit for the Convair Division of General Dynamics Corporation. This investigation was conducted during the period of September 12 to 23, 1960.

The Pye Wacket is being developed as a short range air-to-air missile with a lenticular body design. This particular design was selected for its omnidirectional launch capabilities. Control of the missile is to be accomplished by control jets flush-mounted on the upper and lower surfaces of the missile's centerline.

The test program was initiated to determine force characteristics and reaction jet influence on missile aerodynamics for the unusual attitudes encountered in omnidirectional launches. Data were obtained at Mach numbers 0.6 to 1.6 for various model attitudes through 180-deg yaw and 9-deg angle of attack.

APPARATUS

TEST FACILITY

The PWT 16-Foot Transonic Circuit is a continuous flow, closed circuit type wind tunnel capable of operating at Mach numbers from 0.5 to 1.6 and total pressures up to approximately two atmospheres. The test section is 16 feet square with perforated walls to allow continuous operation through the Mach number range with a minimum of wall interference. Figure 1 shows a sketch of the test section with the model and sting support system and a detail of the test section wall liner plates. A more complete description of the test facility can be found in Ref. 1.

TEST ARTICLE

Two 1/3-scale Pye Wacket models were tested in the 16-Foot Transonic Wind Tunnel. The size of the model prevented the use of a single model to obtain control jet aerodynamic interference effects and force measurements simultaneously.

Manuscript released by authors November 1960.

A view of the sting-mounted force model in the test section is shown in Fig. 2. Figure 3 is a dimensional sketch of the model including the location of the control jets which were installed on the pressure model only. Both the force and the pressure models had the same external dimensions and were constructed so that they could be sting-mounted in either of three mounting positions to provide a wide range of yaw attitude. Figure 3 shows the three sting attachment locations that are called out as 0, 90, and 180-deg mounting positions. The models were mounted in the tunnel with the model pitch plane in the horizontal plane of the test section.

Figure 4 shows a sketch of the force model with a fixed axis system and arrows to indicate the positive directions of forces, moments, and angles.

INSTRUMENTATION

The force model was mounted on a six-component internal strain gage balance. The balance was 1.5 inches in diameter and measured forward and aft normal forces, forward and aft side forces, rolling moment, and axial force. The balance static load components were supplied to the test facility computer by analog-to-digital converters. The model dynamics were monitored on a direct writing oscillograph.

The pressure model was instrumented with 86 static orifices on the upper surface, five total pressure orifices on the leading edge, and six base pressure orifices. Since both the force and pressure models had the same dimensions and were tested at the same conditions, the base pressures from the pressure model were considered applicable to the force model. Figure 5 is a sketch of the pressure model showing the location of all pressure orifices.

The pressure model had two high-pressure air jets to simulate reaction control. Jet chamber pressures and temperatures were measured to determine the jet air weight flows. Figure 6 is a photograph of the instrumented side of the pressure model yawed 180 deg and shows the location of the jets.

TEST DESCRIPTION

TEST PROCEDURE AND CONDITIONS

Force and pressure data were obtained for the models at Mach numbers from 0.6 to 1.6. Both models were tested at yaw angles between 0 and 180 deg and angles of attack from 0 deg

to 9 deg in 3-deg increments. Since the models were mounted with the pitch plane of the model in the horizontal plane of the tunnel, angles of attack were set manually by a sting knuckle joint arrangement. Model yaw angles were obtained remotely by the tunnel sting pitch mechanism. The tunnel sting pitch mechanism allows a maximum of ±12-deg deflection in the vertical plane. The model was mounted on an 11-deg bent sting as shown in Fig. 1 to obtain the maximum yaw range. By pitching the sting from -11 to +12 deg, positive yaw angles of 23 deg could be obtained at each model attachment position. By mounting the model on the sting at the 0-deg mounting position and pitching the sting from -11 to +9 deg, model yaw angles of 0 to 20 deg were obtained. To obtain 90 to 100-deg yaw angle, the model was mounted at the 90-deg mounting position, and then, by rolling the model 180 deg on the sting, 70 to 90 deg of yaw were obtained. By mounting the model at the 180-deg mounting position, yaw angles of 160 to 180 deg were obtained.

The convention used to obtain model yaw angles through 180 deg was not the standard aerodynamic convention usually followed. To obtain 180 deg of yaw with the Pye Wacket missile, the model was first pitched to an angle of attack and then rotated in the "x-y" plane of the model through 180 deg (see Fig. 4). Therefore, at a positive angle of attack and a model yaw angle of 180 deg, the model was actually in a nose down attitude.

Aerodynamic force and moment coefficients were calculated from the model pressure measurements. To calculate these coefficients, each of the surface pressure orifices (1 to 86) were area weighted by dividing the pressure model planform area into triangular and trapezoidal sectors with pressure orifices as the vertices for all the areas. A numerical integration process was then used to calculate the aerodynamic coefficients. Both a positive and negative angle of attack data point were required to obtain these coefficients for the model, since only one surface of the model was pressure instrumented.

The original test plan called for data to be taken at a maximum possible dynamic pressure over the Mach number range. Since the tunnel operating limit was higher than the limit on the balance normal-force gages at 9-deg angle of attack, the balance was the limiting factor. Operating conditions were therefore determined during the first night of testing by monitoring the normal-force readout and bringing the tunnel total pressure up to condition. With the model mounted in the 180-deg position, the axial-force gage was the limiting factor for maximum operating loads. The

tunnel was therefore operated at a lower free-stream dynamic pressure for this mounting position. Shown in Fig. 7 is the variation of both free-stream dynamic pressure and Reynolds number per foot for the 0, 90, and 180-deg mounting positions.

CORRECTIONS

Angle of attack was corrected for sting and balance deflections but not for model misalignment with the flow. The sting and balance deflections were determined by statically loading the balance after it was installed in the test section.

No correction has been made for tunnel wall interference since these effects are believed to be insignificant because of the wave attenuation properties of the perforated walls and the small size of the model. The blockage ratio of this model was 0.163 percent based on the maximum cross sectional area at 0-deg angle of attack.

PRECISION OF MEASUREMENTS

An estimate of the probable error in the computed coefficients and tunnel parameters is shown in Table 1. Assuming the error distribution to be near normal for each measured quantity, the probable error in the final result can best be represented by combining the uncertainty interval of each independent quantity to determine the "propagation of errors" effect. Thus, if $X = f(a, b, c)$, the probable error ΔX is

$$\Delta X = \pm\sqrt{\left(\frac{\partial X}{\partial a}\epsilon_a\right)^2 + \left(\frac{\partial X}{\partial b}\epsilon_b\right)^2 + \left(\frac{\partial X}{\partial c}\epsilon_c\right)^2}$$

where a, b, and c are measured quantities, and ϵ_a, ϵ_b, and ϵ_c are the uncertainty intervals of each measured quantity. A complete description of this method can be found in Ref. 2.

Since the data are single-sample measurements, the probable errors in Table 1 are estimates rather than results of statistical theory. It is estimated that the uncertainty interval based on 95 percent probability will give the true value of the parameters within the range quoted in Table 1.

RESULTS AND DISCUSSION

FORCE CHARACTERISTICS

All force characteristics presented in the following discussion were obtained without jet-control flow. The variation of normal-force coefficient with angle of attack is presented in Figs. 8 and 9. These data are presented for yaw angles of 0, 90, 180 deg only. Figure 8 shows little variation in normal-force coefficient at yaw angles of 0 and 90 deg. As shown in Fig. 9, the normal-force coefficient data at ψ = 180 deg has a different trend at the subsonic Mach numbers. Normal-force coefficients of opposite sign to that normally expected at Mach numbers of 0.6 and 0.8 and positive angles of attack were obtained. No data were obtained at negative angles of attack because of model symmetry. Based on model symmetry with the model at 180 deg of yaw and at a Mach number of 0.8, there must be an abrupt change in normal-force coefficient between +3 and -3-deg angle of attack. At a Mach number of 0.8, angle of attack of 0 deg, and model yaw angle of 180 deg, severe model dynamics were experienced, and no force data could be obtained. By changing the angle of attack or decreasing angle of yaw, the high model dynamics were completely eliminated.

As shown in Figs. 10 and 11 data from the pressure model explain results obtained at ψ = 180 deg. Figure 10 presents an average centerline pressure coefficient distribution taken from three longitudinal pressure rows (see Fig. 5) closest to the centerline of the model. This figure compares an upper and lower surface distribution for ψ = 0 and 180 deg, 0.8 Mach number and 3.2-deg angle of attack. At the ψ = 0 deg position the upper surface is at a lower pressure level than the lower surface, which indicates a positive normal force as was obtained with the force model. With the model at ψ = 180 deg, the flow has separated from the upper surface. Integration of the pressure distributions indicated a negative normal force.

Figure 11 is a similar comparison at Mach number 1.0 and shows the same trend as the Mach number 0.8 plot for the ψ = 0-deg position. At ψ = 180 deg the flow has partially attached to the upper surface, resulting in a positive normal force.

The variation of pitching-moment coefficient with angle of attack is presented in Figs. 12 and 13 for yaw angles of 0, 90, and 180 deg. (All pitching-moment data were taken about the y-axis passing through the geometric center of the model planform.) As shown in Fig. 12, an increase in angle

of attack produces an increase in positive pitching-moment coefficient for the 0-deg yaw position. At the 90-deg yaw position, the center of pressure falls either on or very close to the pitch axes, and very little pitching moment was experienced. At the 180-deg yaw position, positive pitching-moment coefficients were obtained at subsonic Mach number, and negative pitching-moment coefficients were obtained for the supersonic Mach numbers as shown in Fig. 13. At a Mach number of 1.0 a very large change in pitching moment occurred similar to the pitch-up found for conventional wings.

The variation of the slope of the normal-force and the pitching-moment curves with Mach number is presented in Figs. 14 and 15, respectively, for 0-deg angle of yaw.

Shown in Fig. 16 is the variation of the center of pressure with both angle of attack and angle of yaw. In this figure the data are presented for yaw angles of 0, 10, and 20 deg only. At the subsonic Mach numbers the center of pressure location is influenced very little by increasing angle of attack. As the Mach number was increased, the center of pressure moved toward the center of the missile. An increase in angle of attack at the higher Mach numbers also moves the center of pressure nearer the center of the missile. The most extensive angle of yaw data were obtained at an angle of attack of 6.4 deg and at Mach numbers of 0.8 and 1.0. Figure 17 shows the location of the model center of pressure for these test conditions. As angle of yaw was increased from 160 to 180 deg, the center of pressure moved forward on the model (downstream) at a Mach number of 1.0.

Presented in Figs. 18 through 20 is the side-force coefficient for various model attitudes and Mach numbers. At Mach number 1.0 and above, the side-force coefficient is positive and reaches a maximum near 90 deg of yaw as would be expected. At the subsonic Mach numbers, the trend of the data indicates that the maximum side-force coefficient occurred at some yaw angle between 20 and 70 deg. Angle of attack is shown as a parameter in Figs. 19 and 20 for Mach numbers of 0.8 and 1.0, respectively. An angle of attack effect is shown for the subsonic Mach number; however, this effect was negligible in comparison to the change in both trend and level between the two Mach numbers.

The variation of yawing-moment coefficient with yaw angle is presented in Fig. 21 for 0-deg angle of attack. At Mach numbers 1.0 through 1.6, the yawing-moment coefficient has the same trend and indicates that the missile has a negative yawing moment through approximately 120 deg of yaw. At Mach numbers 0.6 and 0.8, the yawing-moment coefficient

is at a different level than at the supersonic Mach numbers and has an abrupt shift near 80-deg yaw angle. Analysis of the base pressure data at the subsonic Mach number shows that the separated flow in the base region at yaw angles near 0 deg attaches to the base as the missile is yawed to approximately 80-deg yaw angle causing the shift in yawing moment. The variation of yawing-moment coefficient with yaw angle is presented in Figs. 22 and 23 for Mach numbers 0.8 and 1.0, respectively, for various angles of attack. These data show little variation in yawing-moment coefficient as angle of attack was increased except near a yaw angle of 80 deg.

The variation of rolling-moment coefficient with angle of yaw is presented for Mach numbers of 0.8 and 1.0 in Figs. 24 and 25, respectively. These data are presented with angle of attack as a parameter and show that an increase in angle of attack causes a considerable increase in rolling-moment coefficient, especially near the 90-deg yaw position.

Figure 26 shows the variation with Mach number of forebody and base-drag coefficients at 0-deg angle of attack and 0-deg angle of yaw. The base-drag coefficient was calculated from base pressure data obtained from the pressure model. Since both the pressure model and the force model were the same configuration and had the same external dimensions, it was assumed that both models would have the same base-drag variations with Mach number. Therefore, the base-drag coefficient from the pressure model was used to correct the force model axial-force data to forebody axial-force coefficient.

JET EFFECTS

The purpose of the pressure phase of this test was to determine the effect of control jets on the aerodynamic forces and moments. The control jets were converging-diverging nozzles with an exit Mach number of approximately 2.7 and a throat diameter of 0.25 in. High pressure air was used as the working fluid with a stagnation pressure of 700 psia and air weight flows of one lb/sec per jet. The aerodynamic forces and moments on the model were calculated by numerical integration of the model surface pressures. Jet reaction forces are not included in the model forces and moments presented. Statements concerning jet effects on the model pertain only to the influence of the jet on the model pressure distributions. No pressure orifices were provided on the model surface opposite the jets, and it was assumed that the jet influence field did not extend to this model surface.

Shown in Figs. 27 and 28 is the effect of the jet flow on the normal-force and pitching-moment coefficients as a function of Mach number at 0-deg yaw angle and 0, 3.2, and 6.4-deg angle of attack. These data are presented as a change (jet-on minus jet-off) in the normal-force and pitching-moment coefficients. Figure 27 shows that turning the upper surface jets on caused a decrease in the normal-force coefficient, or essentially, the aerodynamic lift on the model is decreased. Turning the lower surface jets on has the opposite effect on the normal-force coefficient, or the lift is increased. Note that this jet influence in both cases augments the jet reaction forces. The calculated normal-force coefficient C_{Nj} caused by the jet reaction force of both jets is shown as the dashed curve on the figures. The aerodynamic interference of the jet is approximately equal to the effect of the jet thrust. The magnitude, of course, would vary depending on the jet characteristics and missile trajectory.

Figure 28 shows that at Mach numbers from 1.0 to 1.6, with the upper surface jets operating (jets-on), an increase in pitching-moment coefficient was obtained, whereas with the lower surface jets operating, a decrease in pitching moment was obtained. At the subsonic Mach numbers, the control jets cause very little change in the pitching-moment coefficient. The calculated pitching-moment coefficient C_{mj} caused by the jet reaction force of both jets is shown by the dashed lines on Fig. 28. With the upper and lower surface jets operating, the aerodynamic interference of the jets is of significant magnitude and results in considerable jet augmentation. As stated previously, the magnitude of these effects is dependent upon jet characteristics and missile trajectory.

The effects of jet flow on the normal-force and pitching-moment coefficients throughout the range of Mach numbers and yaw angles are presented in Figs. 29 and 30, respectively. These data are for $\alpha = 0$ deg with only the upper surface control jets in operation. The predominant changes in coefficients occur generally between M = 0.8 and 1.0 and are essentially similar for a range of ψ of ±20 deg about $\psi = 0$, 90, and 180 deg.

Figure 31 shows the effect of varying jet pressure ratio on the normal-force and pitching-moment coefficient. Limited data were obtained for various chamber pressures, but it is interesting to note that at a Mach number of 1.2 ($\alpha = 0$ and $\psi = 0$) the jet thrust and aerodynamic effects are essentially the same magnitude and have the same trends for both normal-force and pitching-moment coefficients.

The effects of the control jet flow on the surface pressure coefficients in the immediate vicinity of a jet are shown in Figs. 32 and 33 for free-stream Mach numbers of 0.6 and 1.4. The change in C_p is very large close to the jets but attenuates rapidly with distance from the jet. The pressures immediately ahead of the jet reach or approach free-stream total pressure, and the pressures immediately behind the jet are very low because of jet-ejector action. These data are typical and show the mechanism through which the aerodynamic influence of the reaction jets results.

CONCLUSIONS

1. The expected levels and trends of normal-force and pitching-moment coefficients were exhibited by the body tested except at yaw attitudes greater than 160 deg.

2. The expected levels and trends of side-force and yawing-moment coefficients were exhibited by the body tested except at yaw attitudes near 80 deg.

3. Unusual stability characteristics existed for the body tested at a reverse attitude. Flow separation, even at low angles of attack, occurred on the reversed body at sonic and lower test velocities. This separation resulted in net body normal forces and pitching moments having opposite direction from those for the attached-flow case.

4. Flow separation and reattachment were encountered on the model at extreme angles of yaw. Associated with these transitional effects were very large shifts in center-of-pressure location.

5. Abrupt changes in yawing-moment coefficients occurred at yaw angles near 80 deg for subsonic Mach numbers.

6. The control effectiveness of the reaction jets was increased as a result of aerodynamic interactions. The magnitude of the interaction on pitching-moment coefficient was approximately the same as the control jet reaction at supersonic speed. The aerodynamic interaction at subsonic speeds was generally negligible.

REFERENCES

1. Test Facilities Handbook, (2nd Edition). "Propulsion Wind Tunnel Facility, Vol. 3." Arnold Engineering Development Center, January 1959.

2. Dean, R. C., Jr. Aerodynamic Measurements. Gas Turbine Laboratory, Massachusetts Institute of Technology, Cambridge, Mass., 1953.

TABLE 1

PRECISION OF MEASUREMENTS

	ψ = 0, 90		ψ = 180	
	$M_\infty = 0.60$	$M_\infty = 1.60$	$M_\infty = 0.60$	$M_\infty = 1.60$
C_N	±0.025	±0.023	±0.045	±0.042
C_A	±0.001	±0.001	±0.002	±0.002
C_Y	±0.004	±0.004	±0.007	±0.007
C_m	±0.007	±0.006	±0.012	±0.011
C_n	±0.001	±0.001	±0.002	±0.002
C_l	±0.002	±0.002	±0.004	±0.003
C_p	±0.009	±0.008	±0.015	±0.014
M_∞	±0.003	±0.007	±0.004	±0.015
q_∞	±4.25	±7.10	±4.17	±7.80

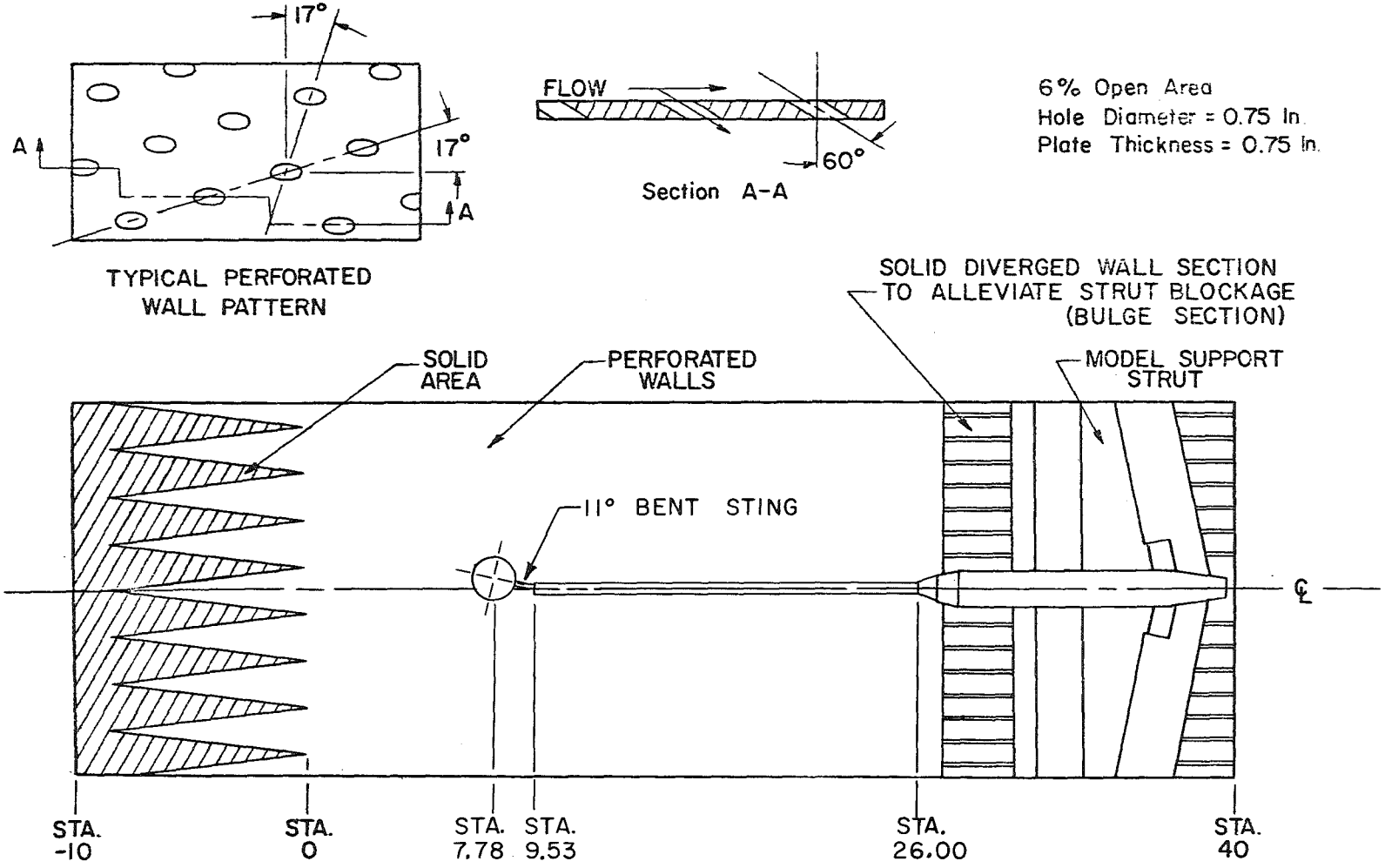

Fig. 1 Model Installation and Details of the Perforated Walls

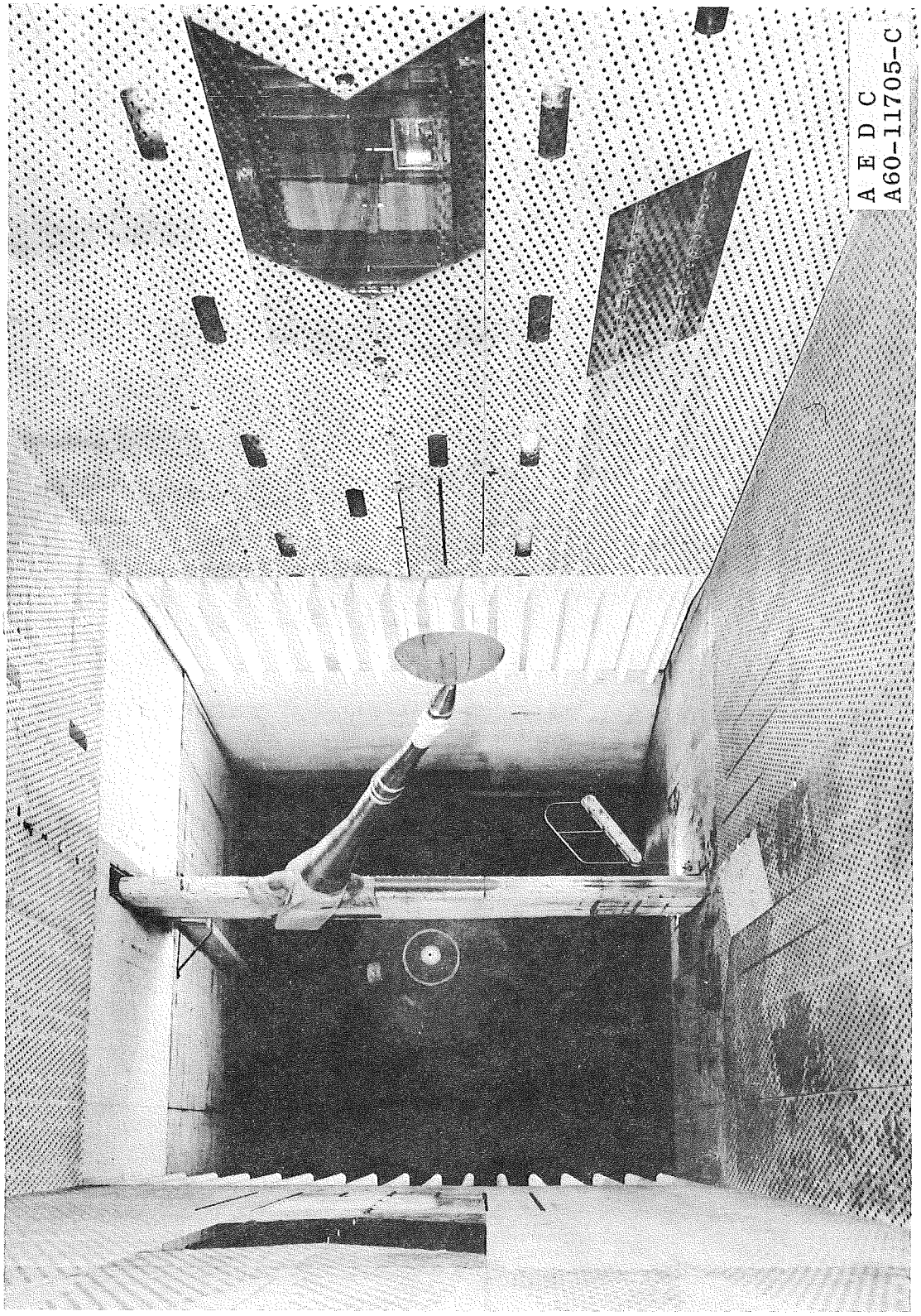

Fig. 2 Pye Wacket Model Installation in the PWT

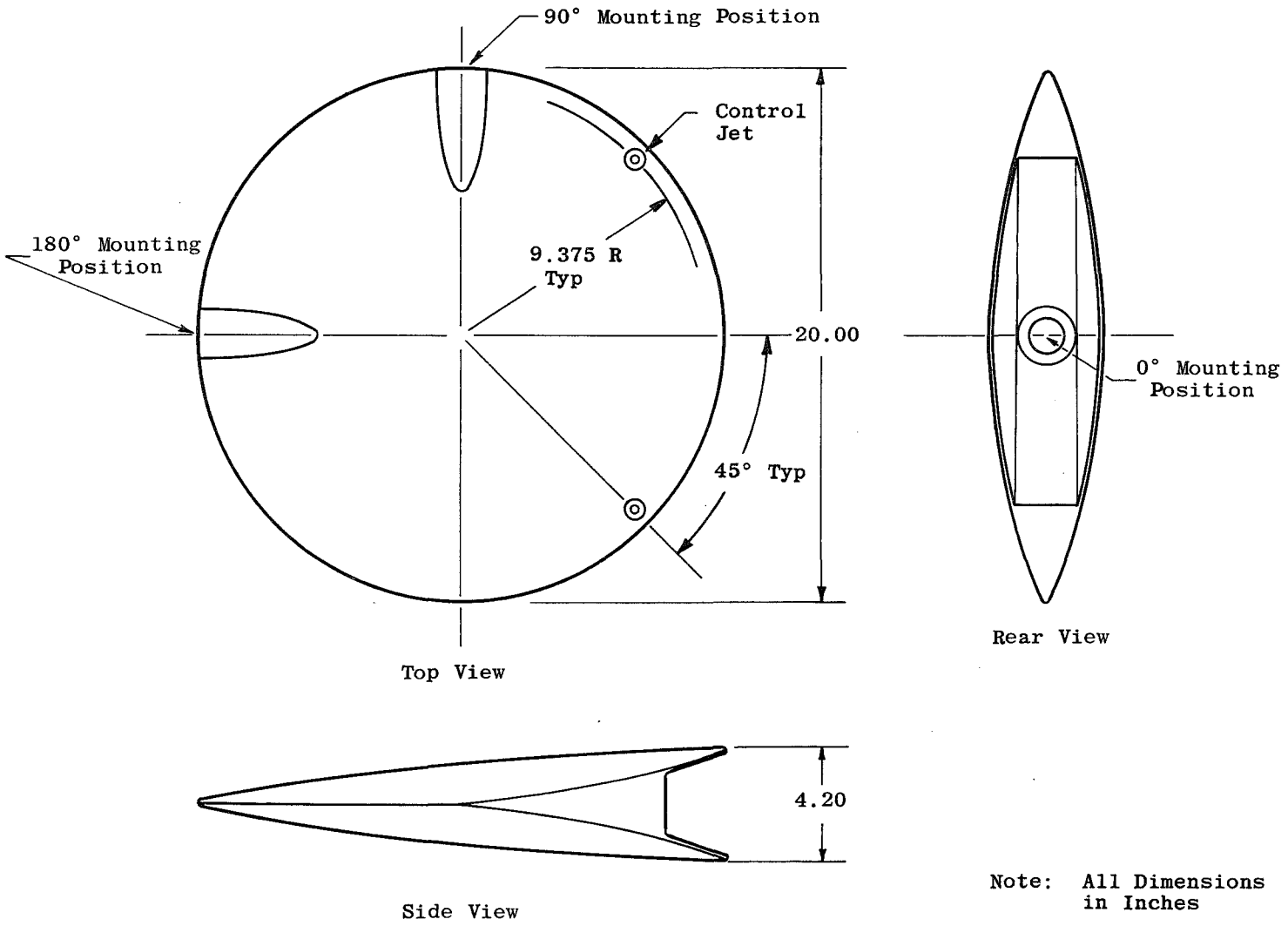

Fig. 3 Model Dimensions

NOTE:

1. Axis System is fixed to and moves with the missle.
2. Arrows indicate positive directions of forces, moments and angles with the exception of yaw angle, ψ. The arrow indicates negative direction of yaw angle.
3. u, v, and w are components of velocity, V.

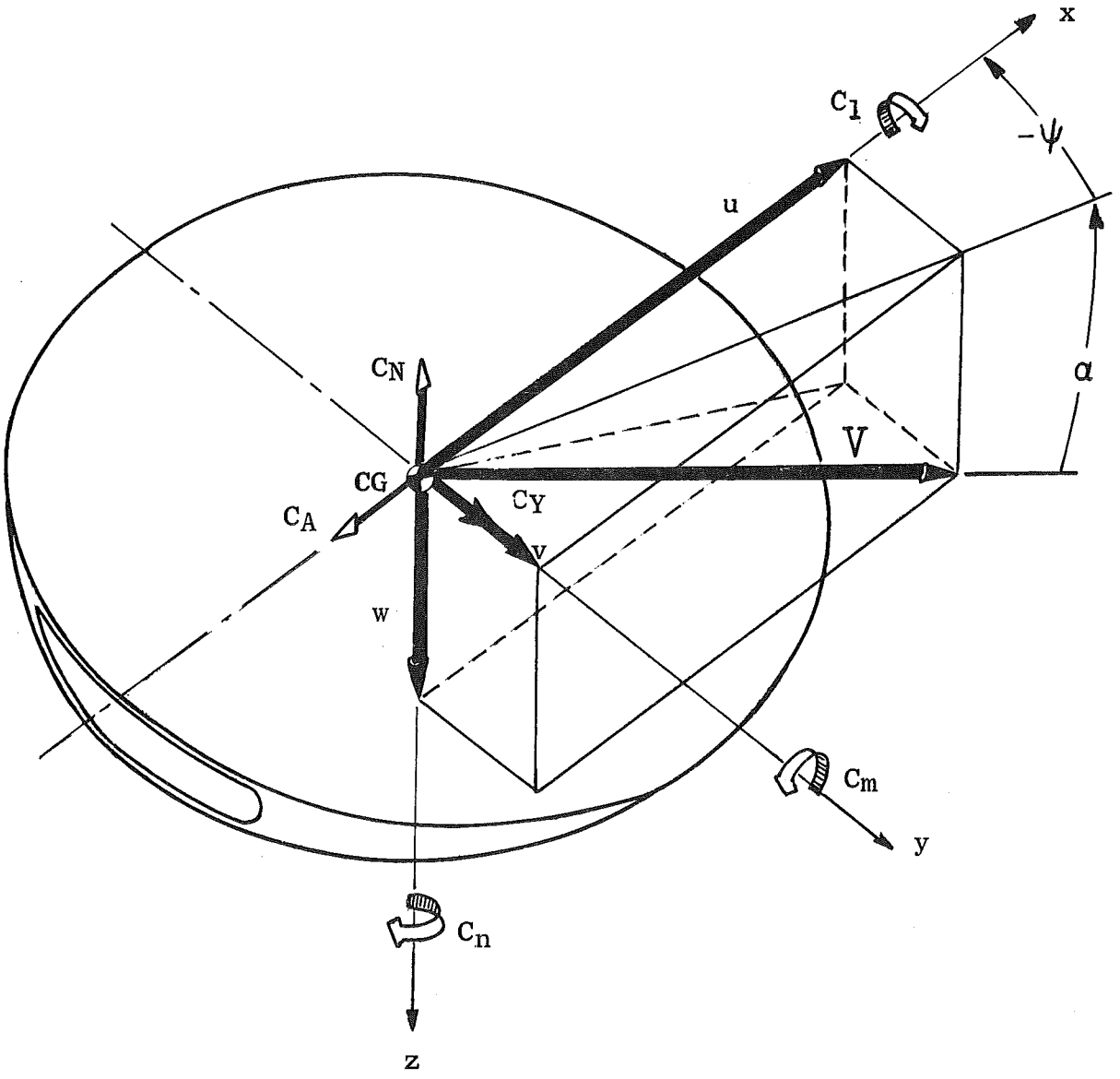

Fig. 4 Model Axis System

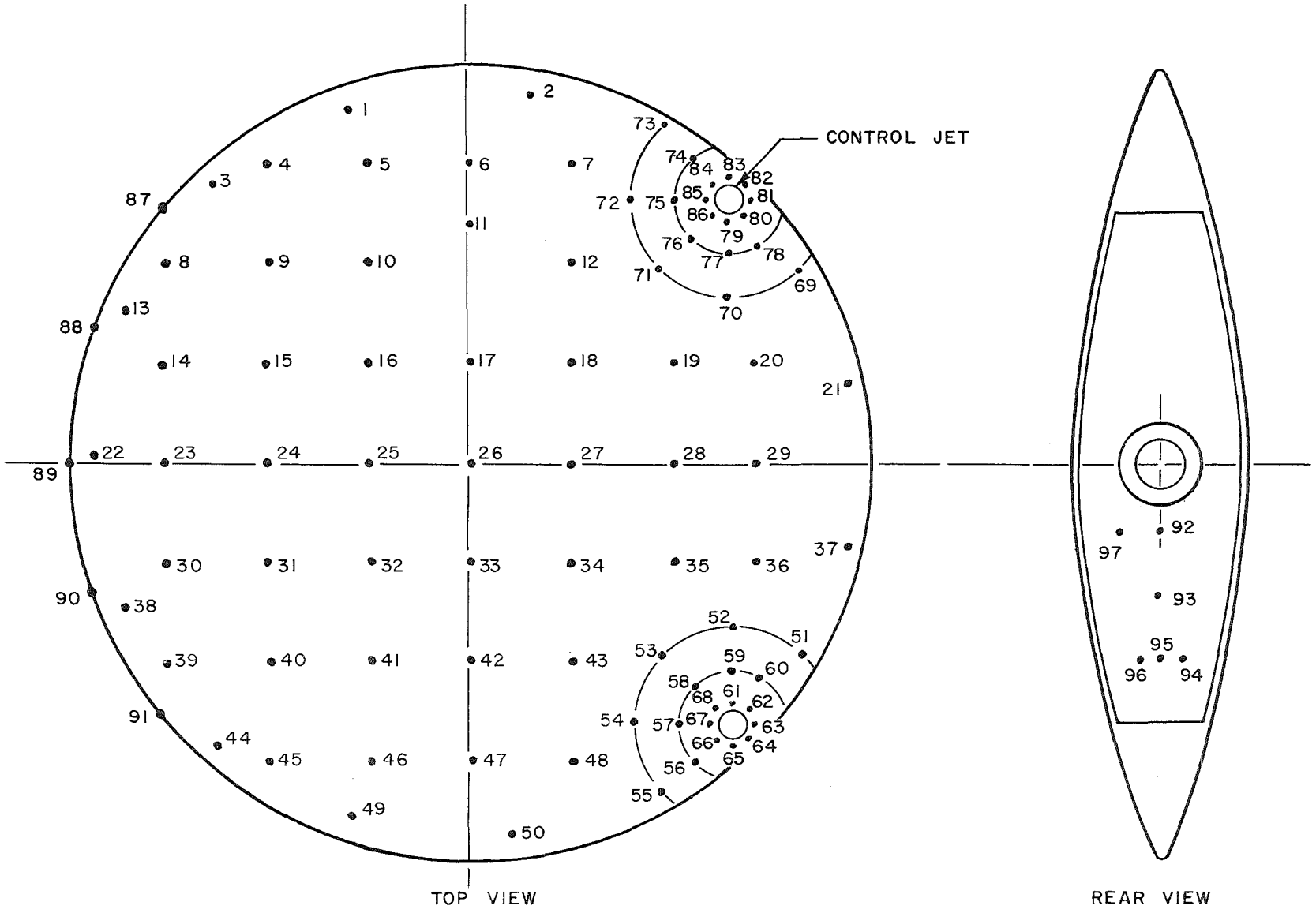

Fig. 5 Pressure Orifice Locations

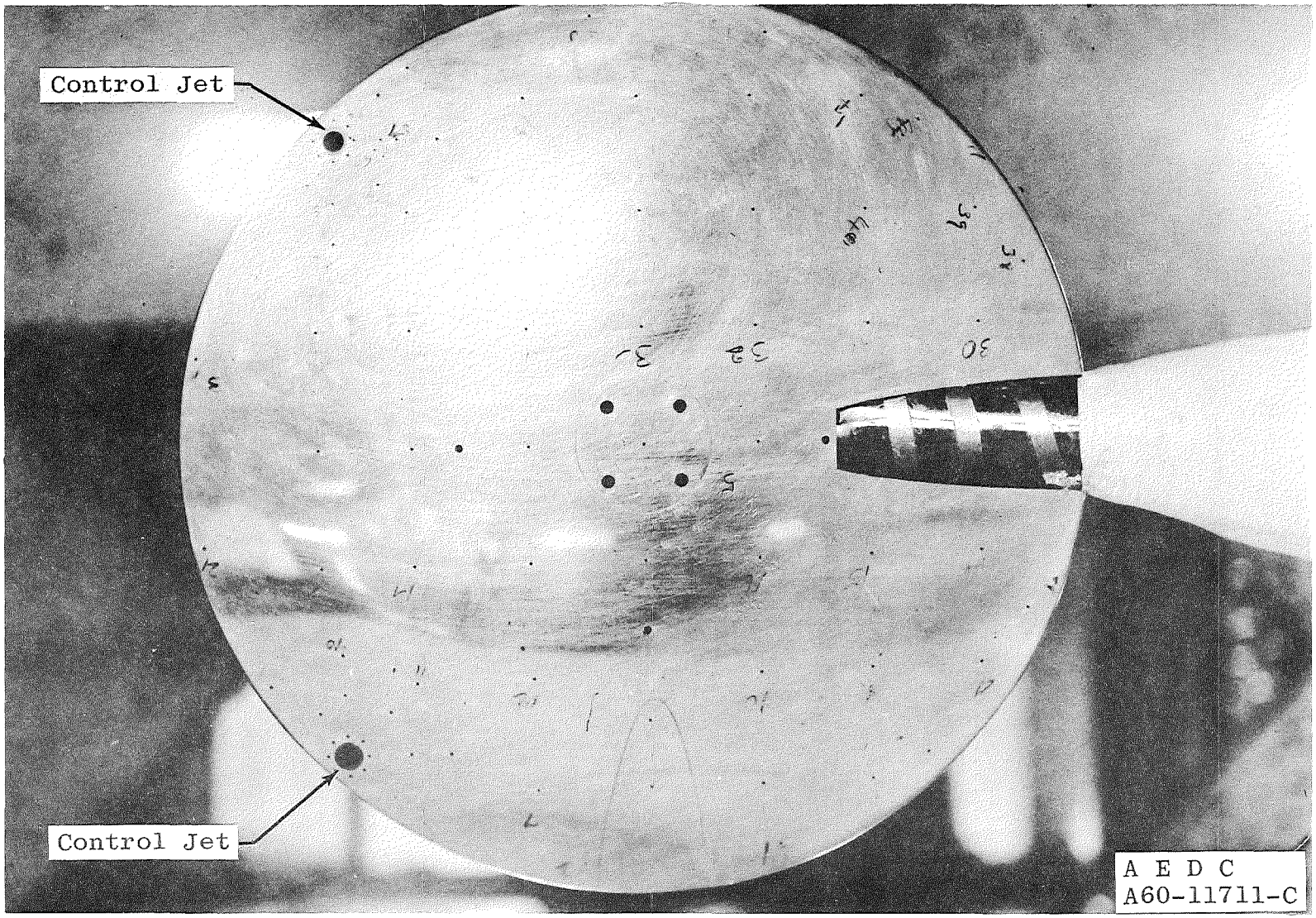

Fig. 6 View of the Instrumented Side of the Model Mounted at the 180-deg Yaw Position

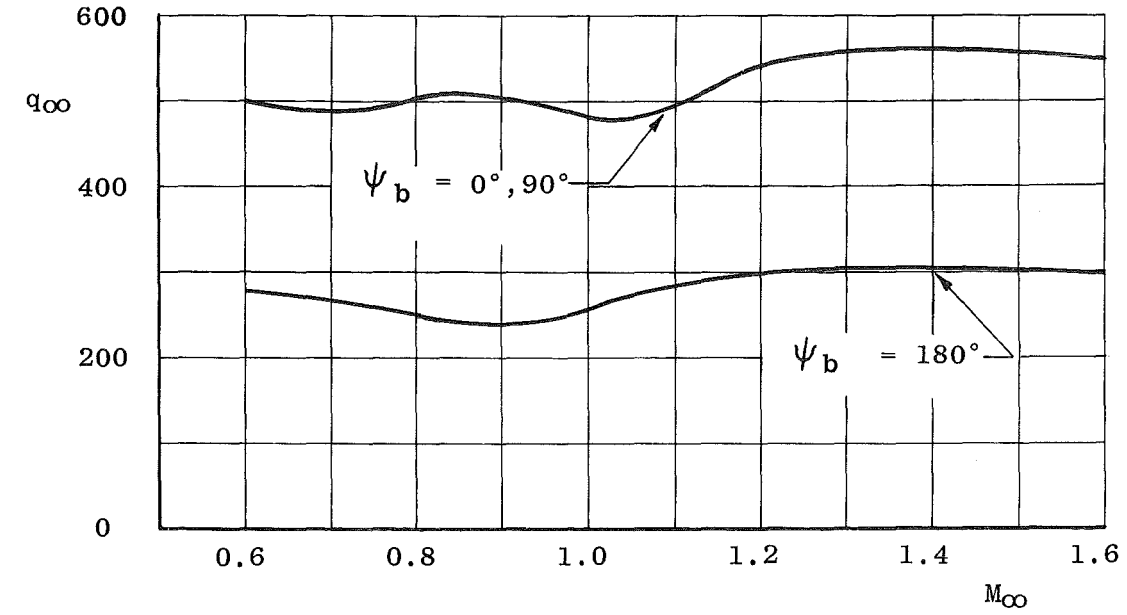

a. Dynamic Pressure

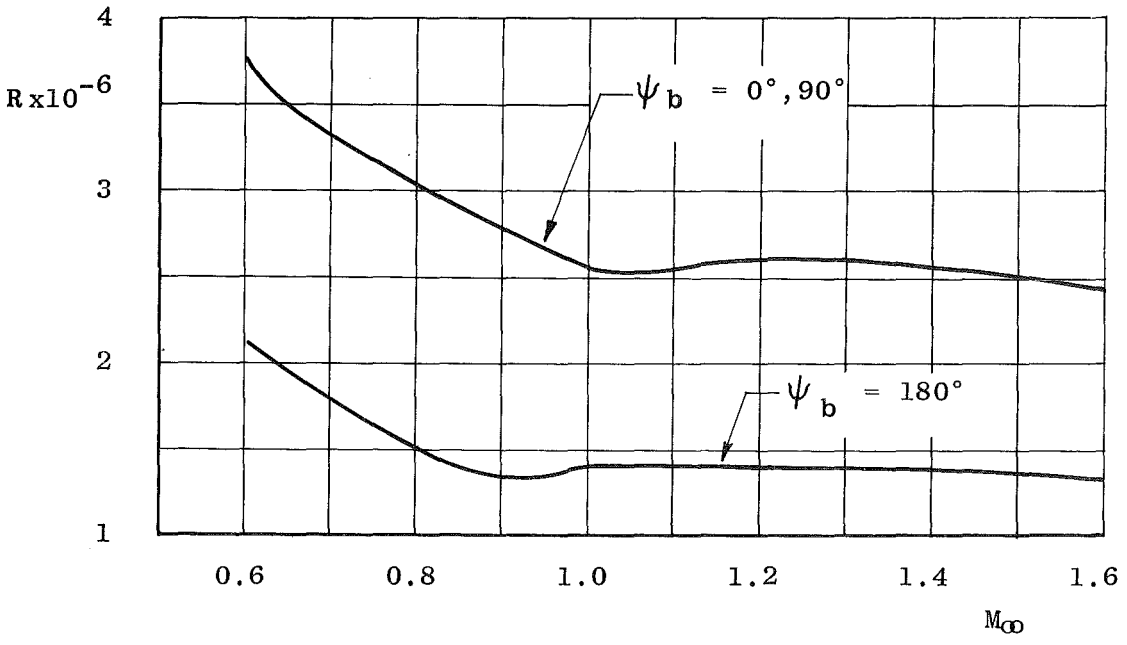

b. Reynolds Number Per Foot

Fig. 7 Test Conditions for the Pye Wacket Model

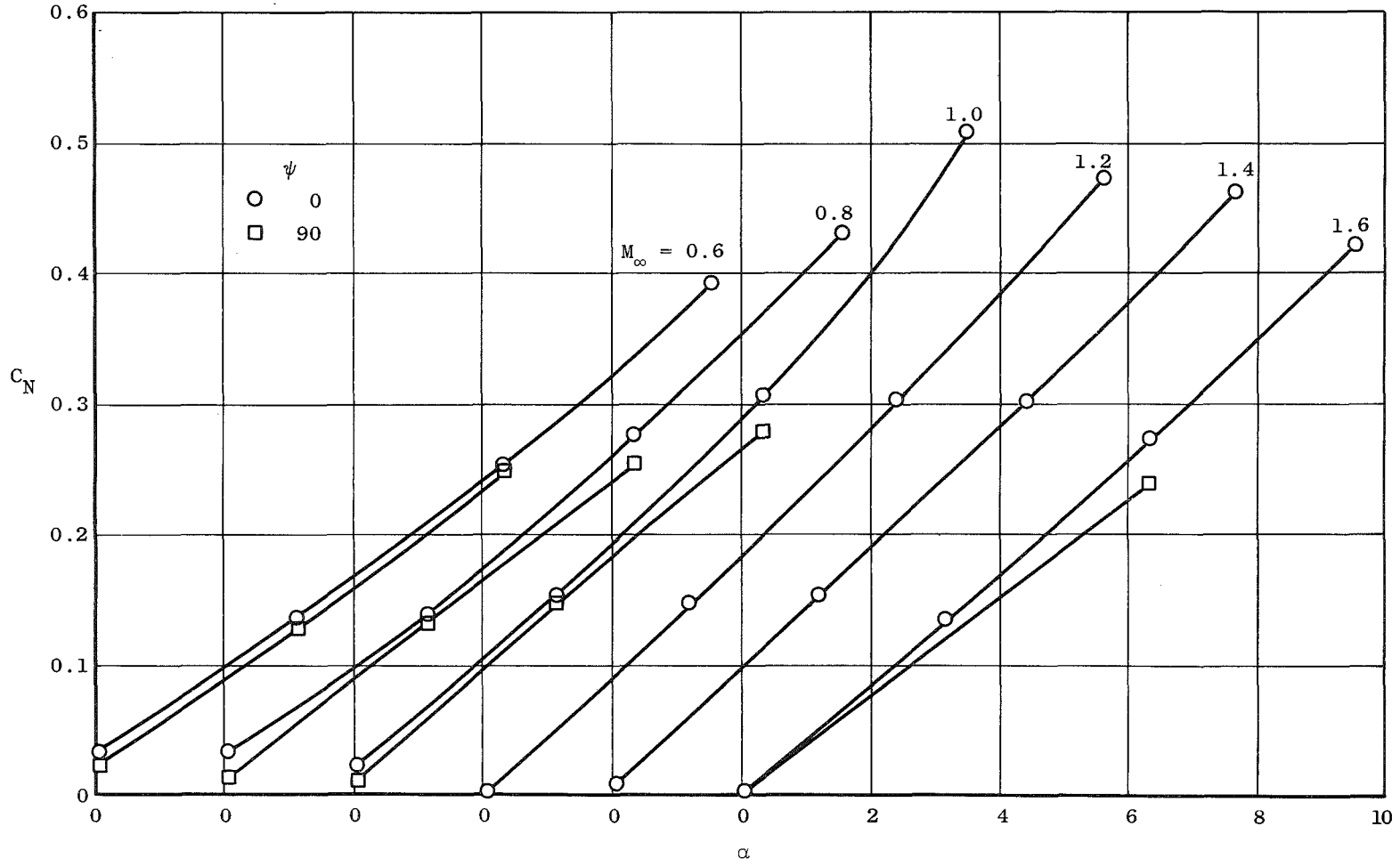

Fig. 8 Variation of Normal-Force Coefficient with Angle of Attack, ψ = 0 and 90

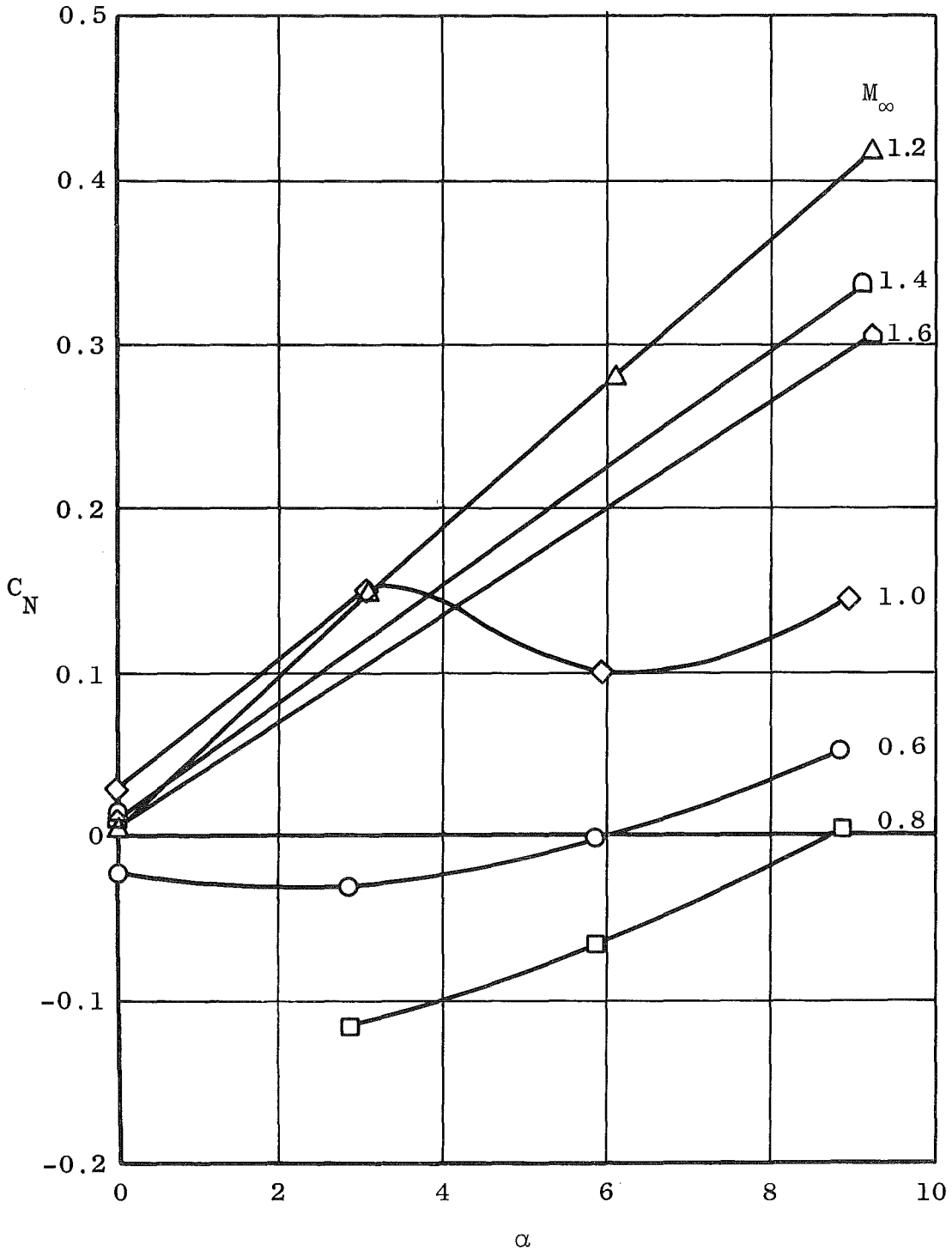

Fig. 9 Variation of Normal-Force Coefficient with Angle of Attack, $\psi = 180$

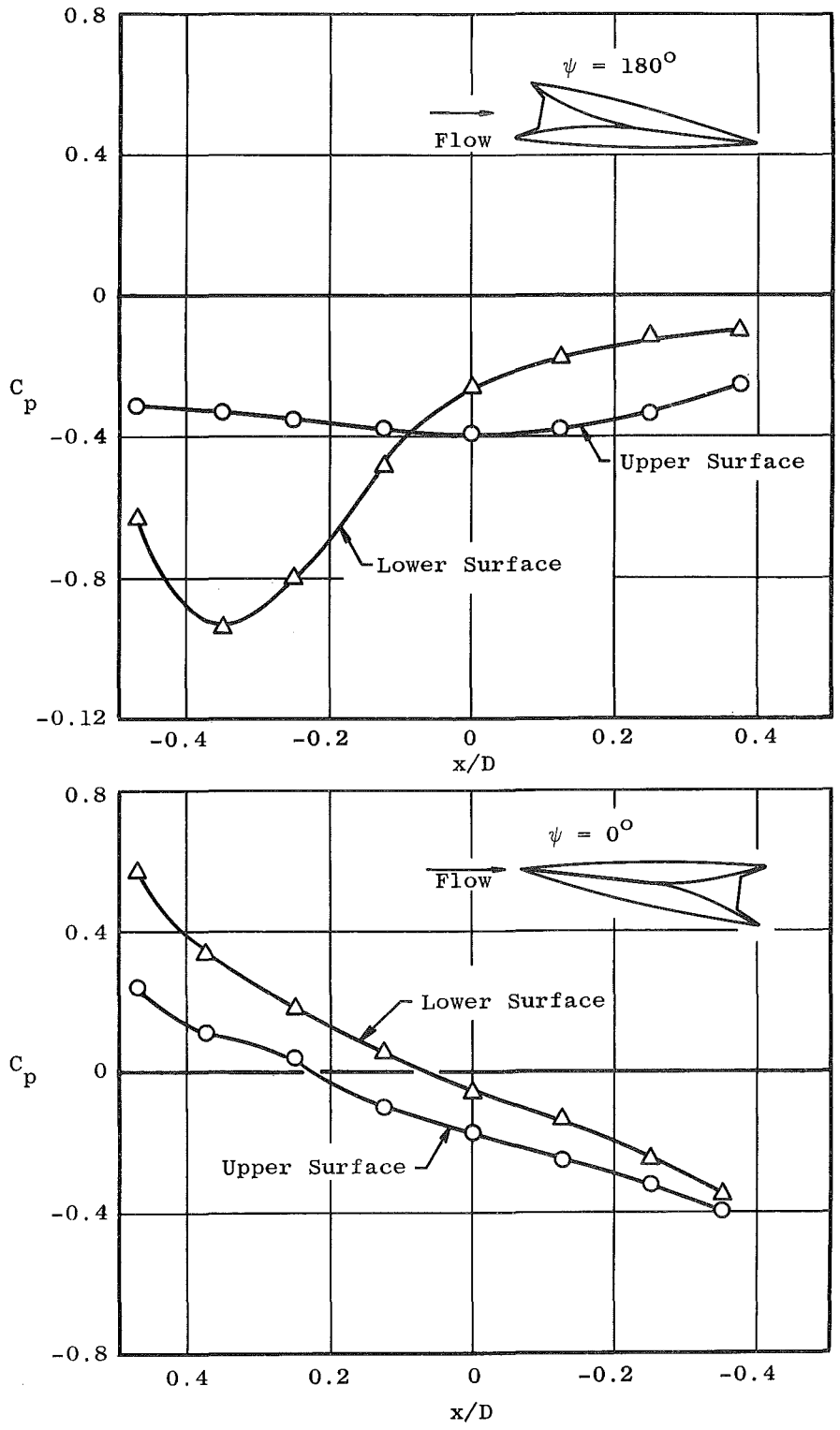

Fig. 10 Model Centerline Pressure Coefficient Distribution, $M_\infty = 0.8$, $\alpha = 3.2$

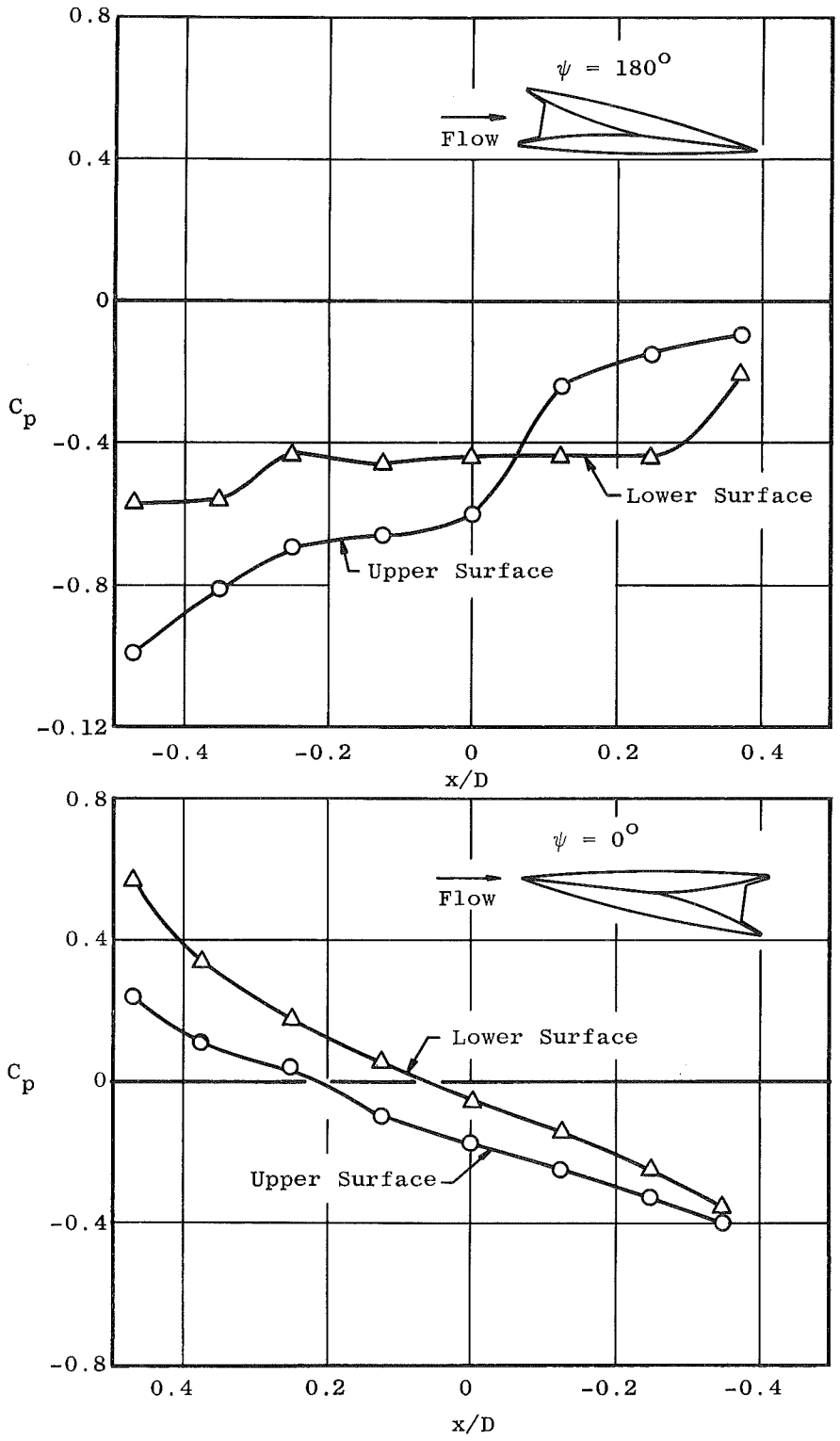

Fig. 11 Model Centerline Pressure Coefficient Distribution, $M_\infty = 1.0$, $\alpha = 3.2$

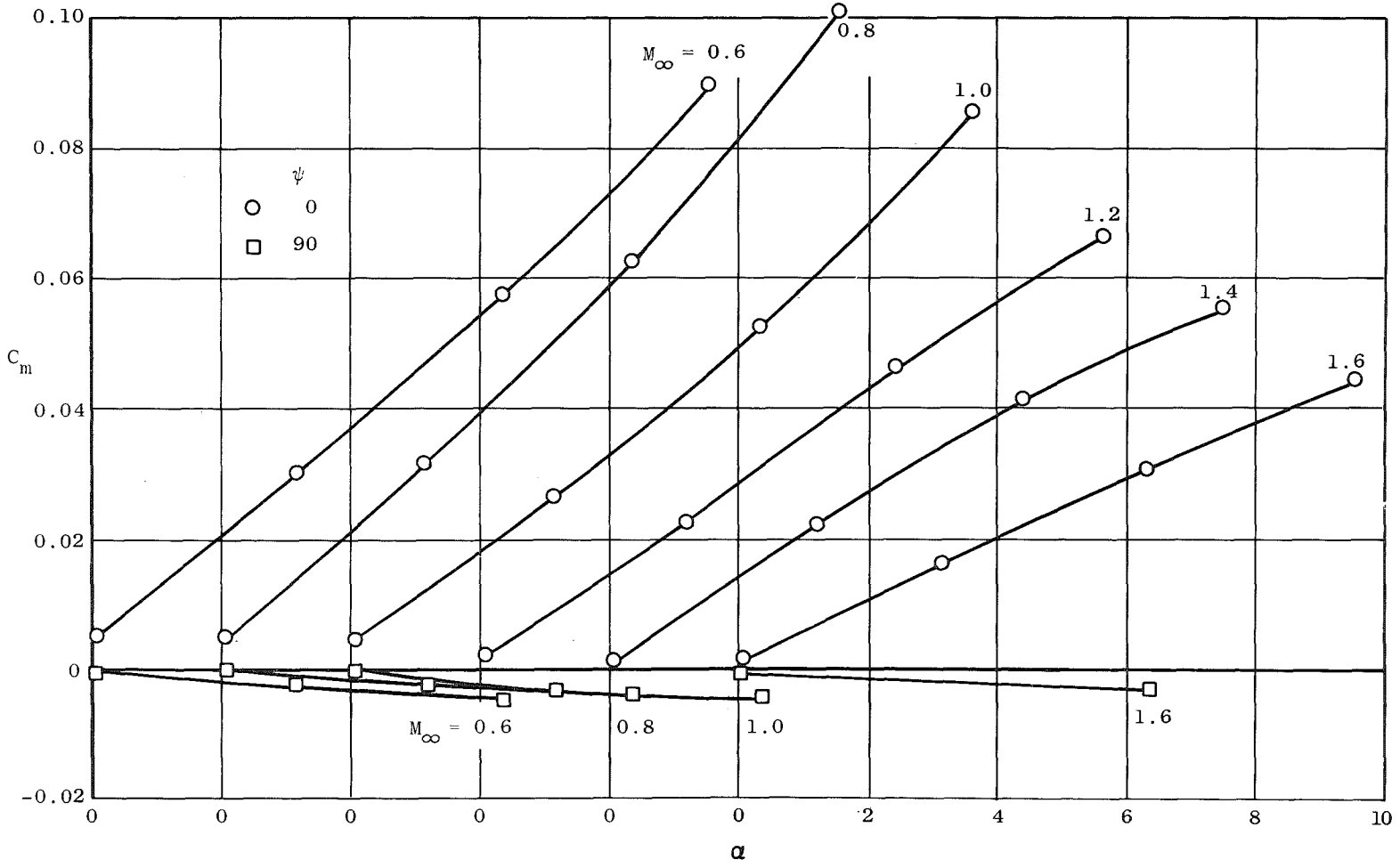

Fig. 12 Effect of Angle of Attack and Mach Number on Pitching-Moment Coefficient, $\psi = 0$ and 90

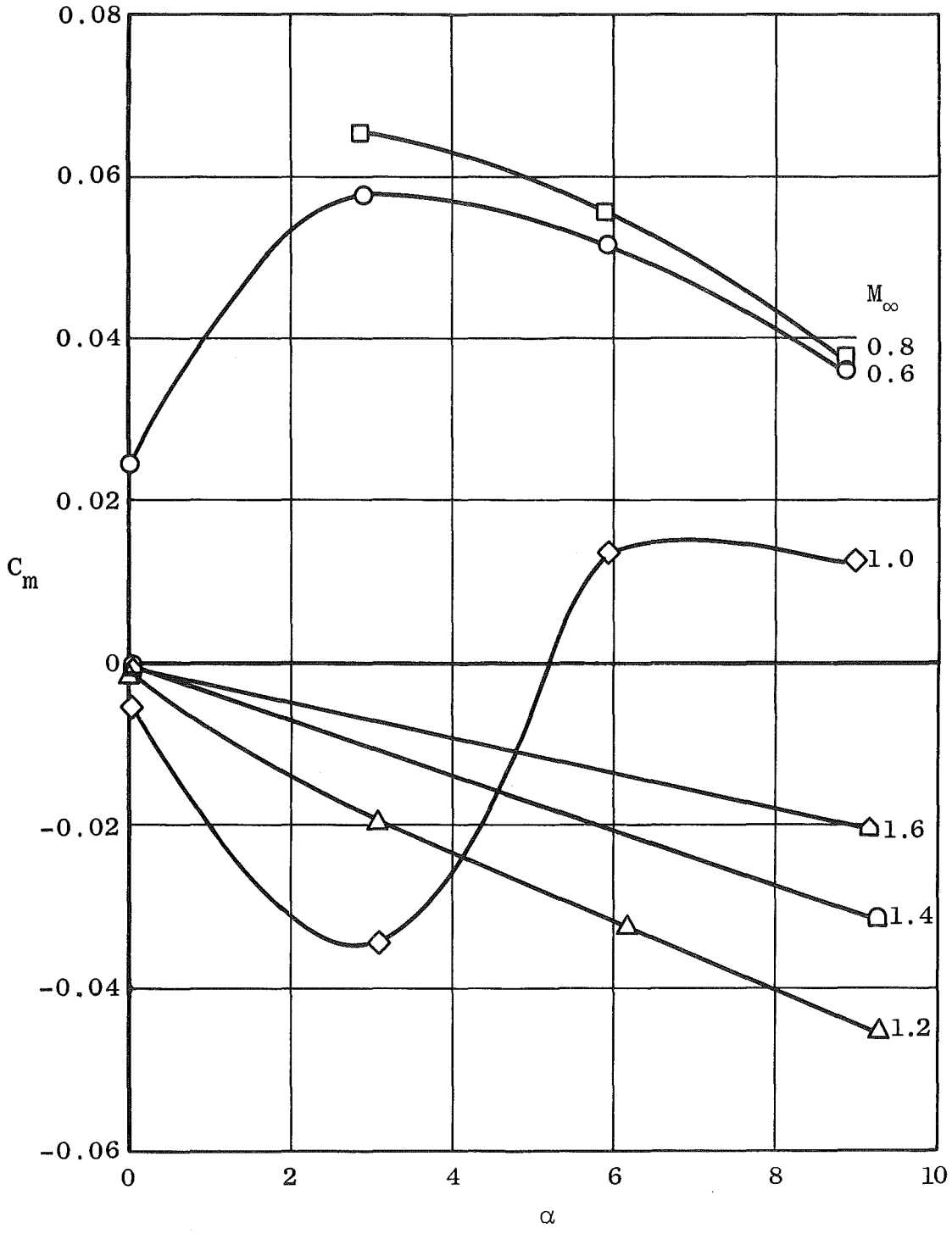

Fig. 13 Effect of Angle of Attack and Mach Number on Pitching-Moment Coefficient, $\psi = 180$

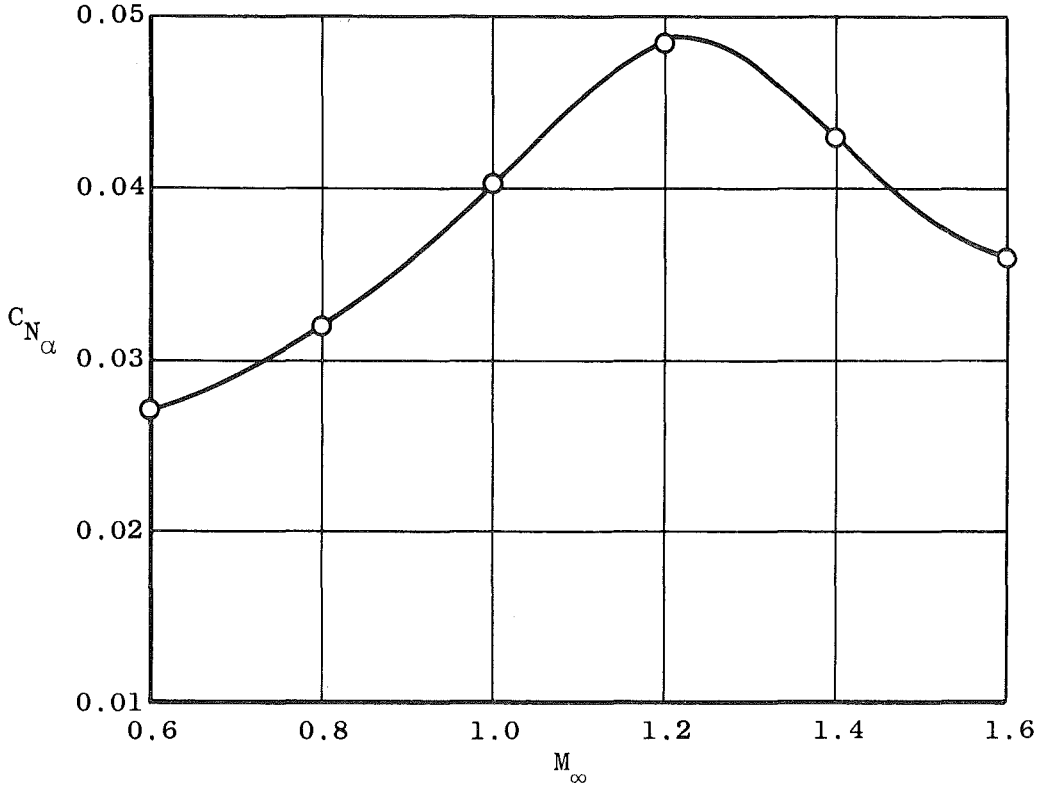

Fig. 14 Variation of Normal-Force Curve Slope with Mach Number, $\psi = 0$

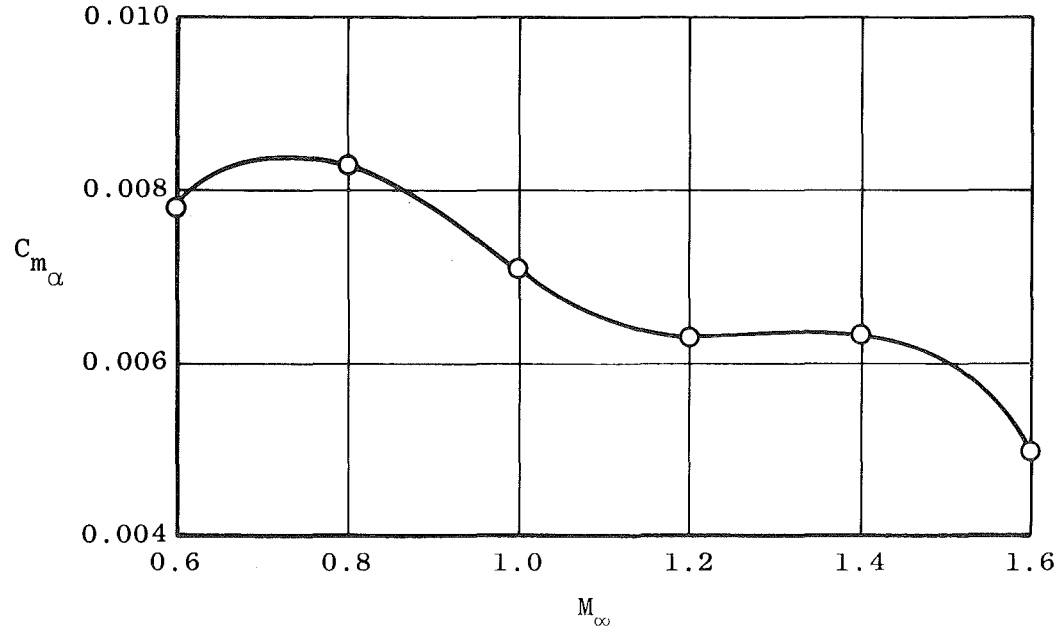

Fig. 15 Variation of Pitching-Moment Curve Slope with Mach Number, $\psi = 0$

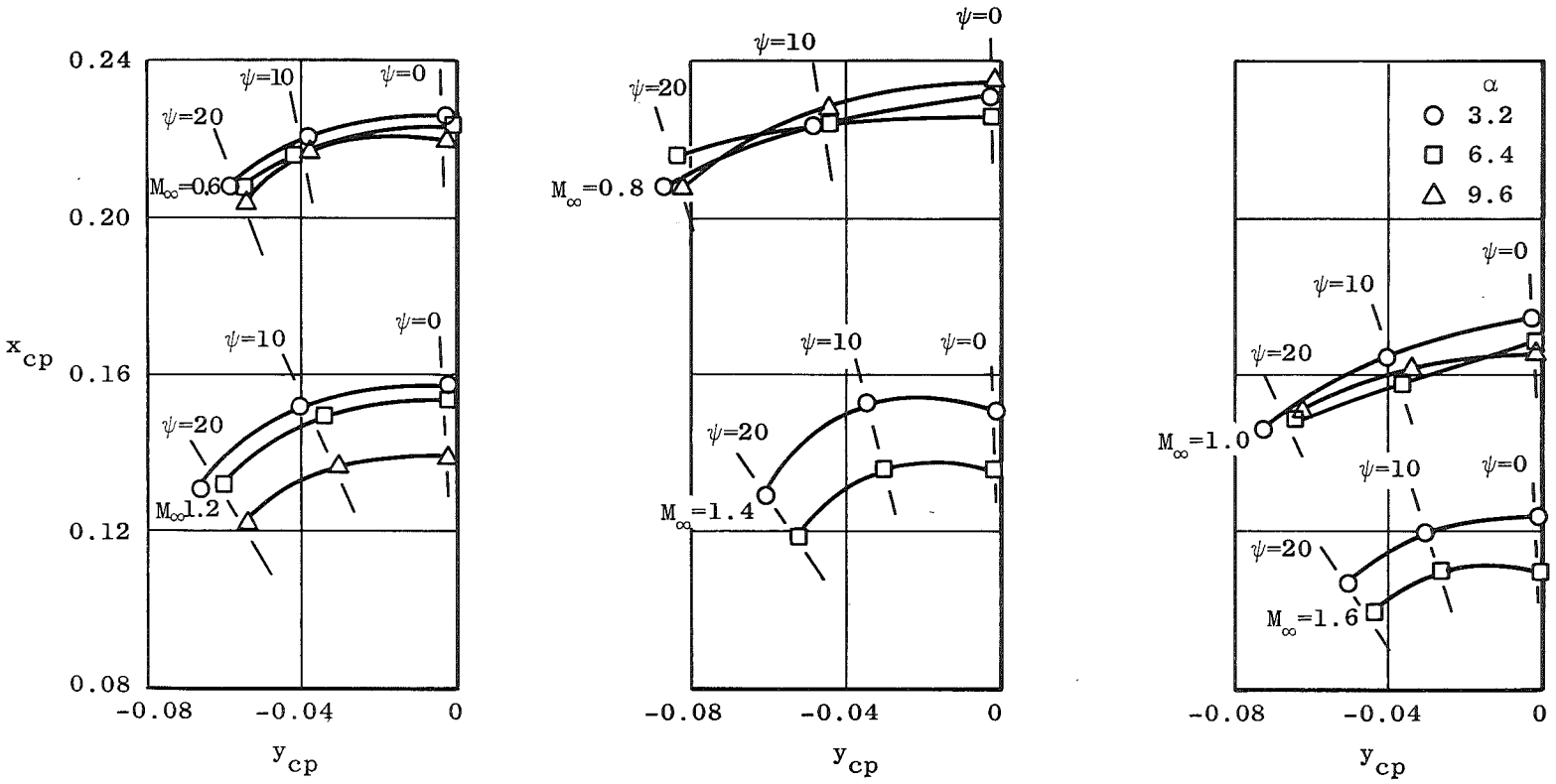

Fig. 16 Effect of Angle of Attack and Angle of Yaw on Center of Pressure Location

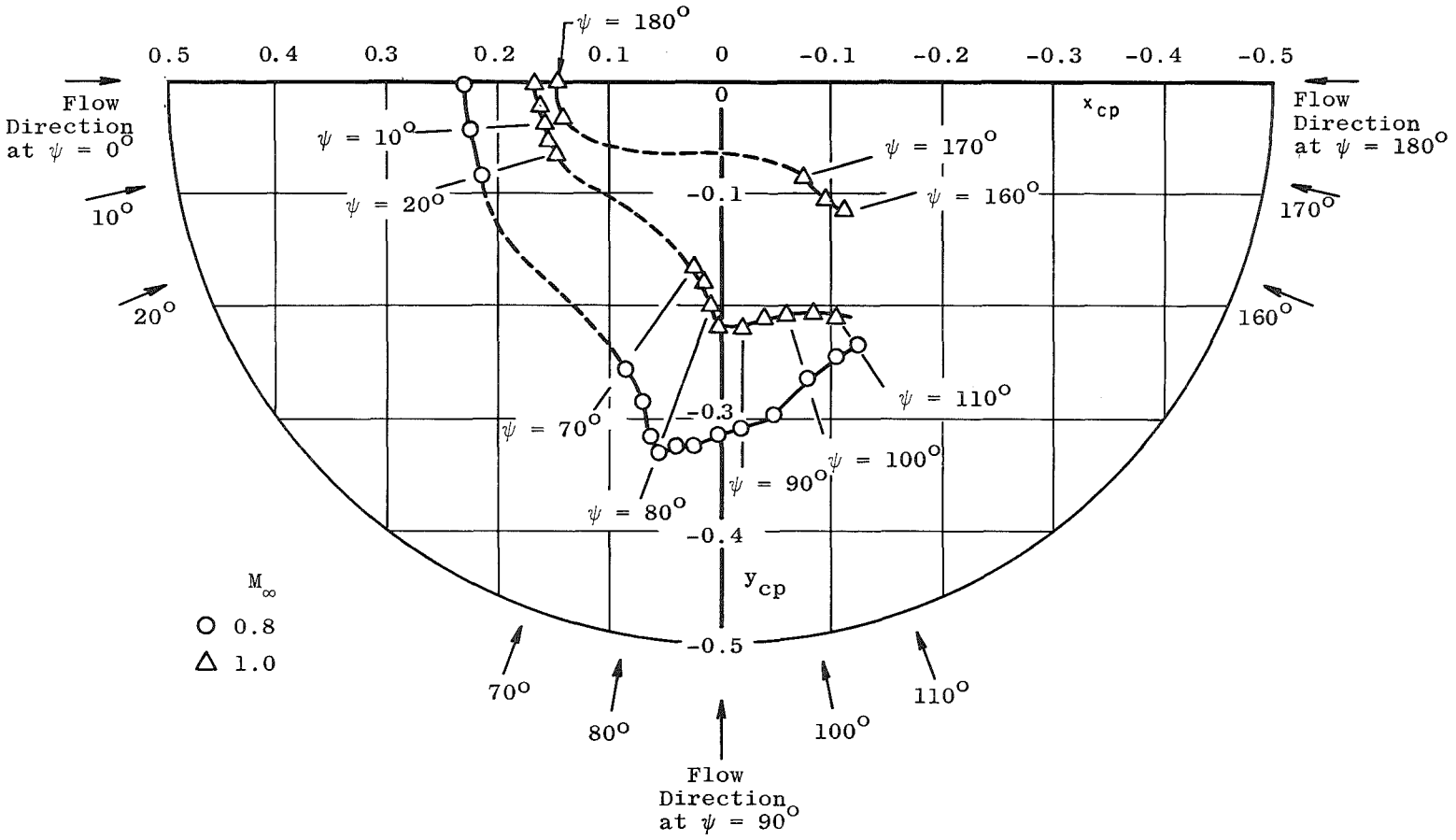

Fig. 17 Effect of Yaw Angle on Center of Pressure Location, $M_\infty = 0.8$ and 1.0, $\alpha = 6.4$

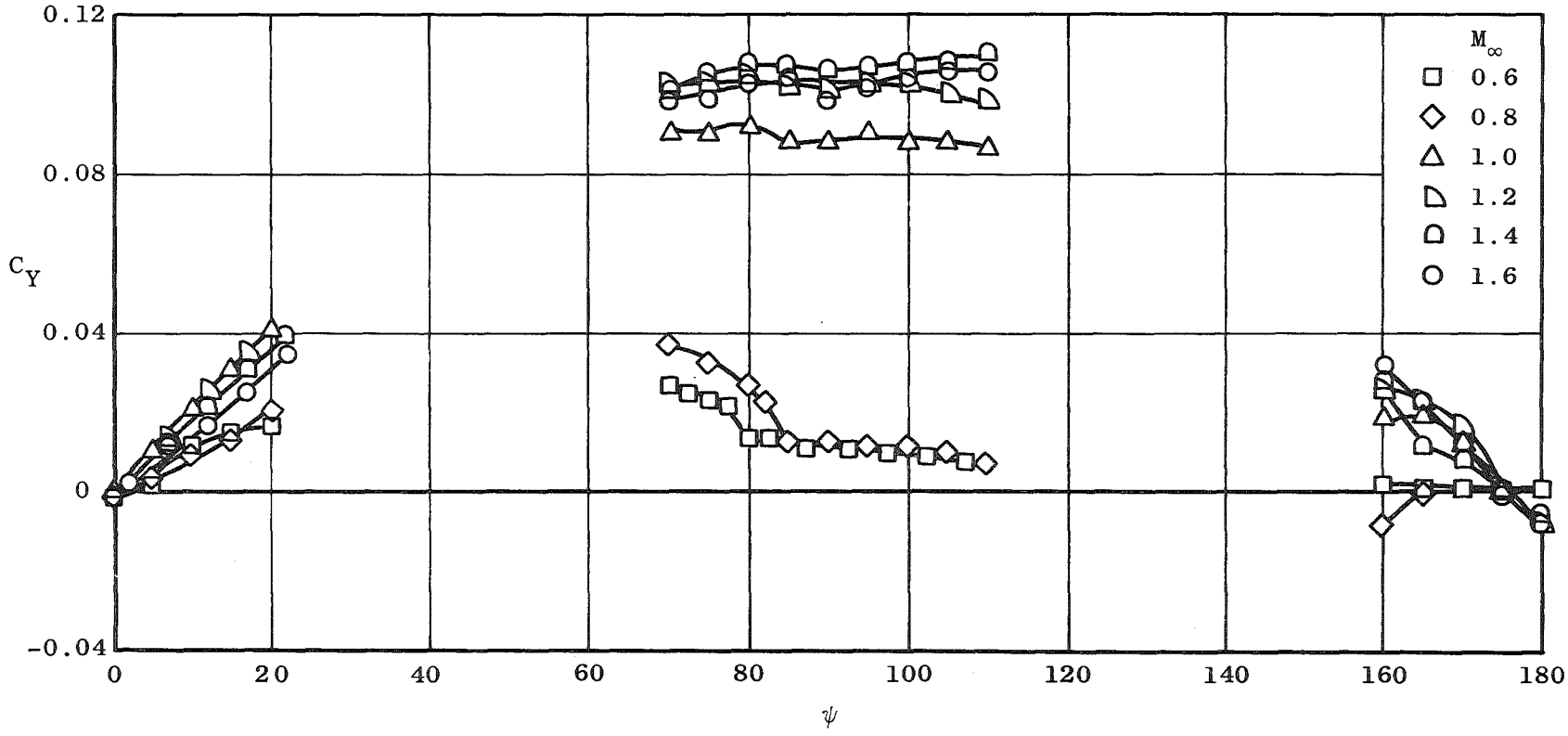

Fig. 18 Variation of Side-Force Coefficient with Yaw Angle, $\alpha = 0$

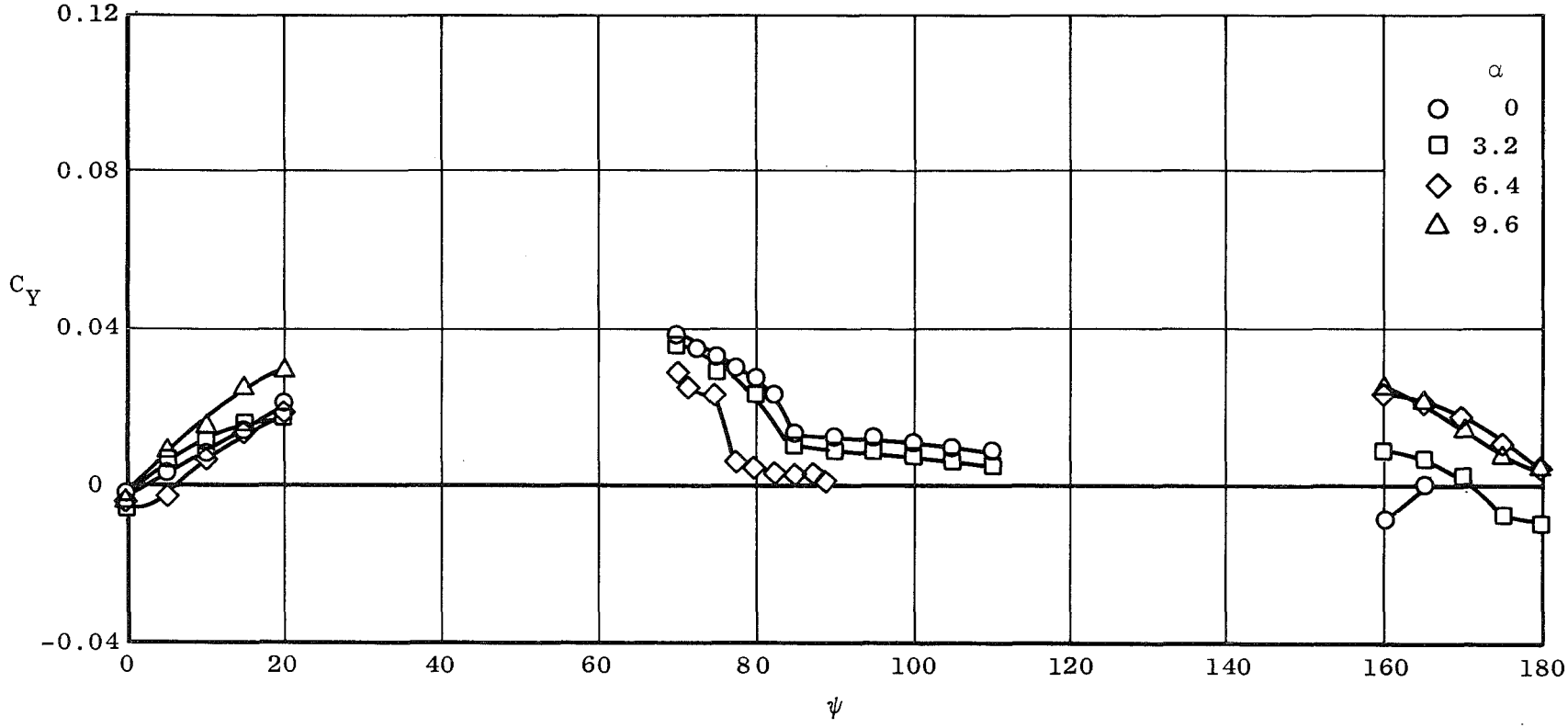

Fig. 19 Variation of Side-Force Coefficient with Yaw Angle, $M_\infty = 0.8$

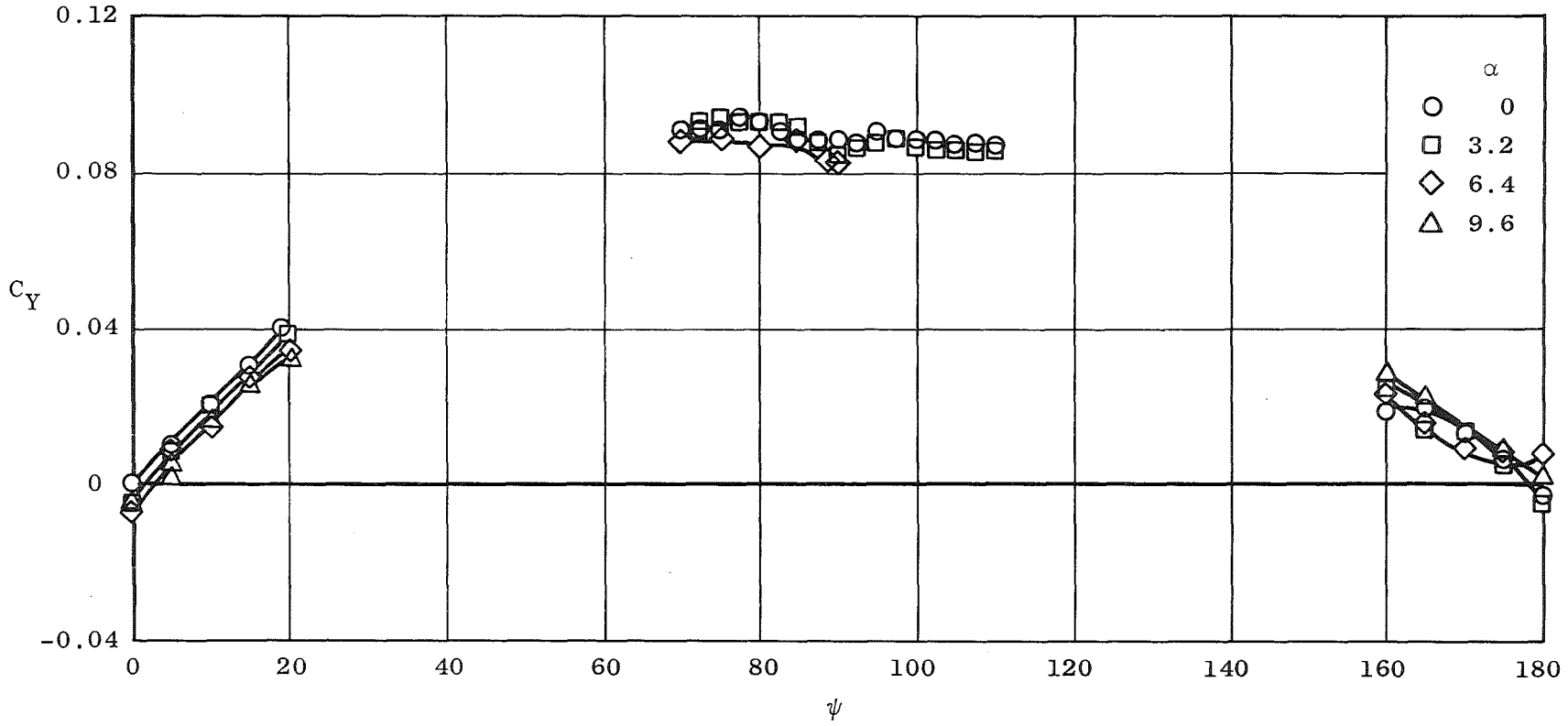

Fig. 20 Variation of Side-Force Coefficient with Yaw Angle, $M_\infty = 1.0$

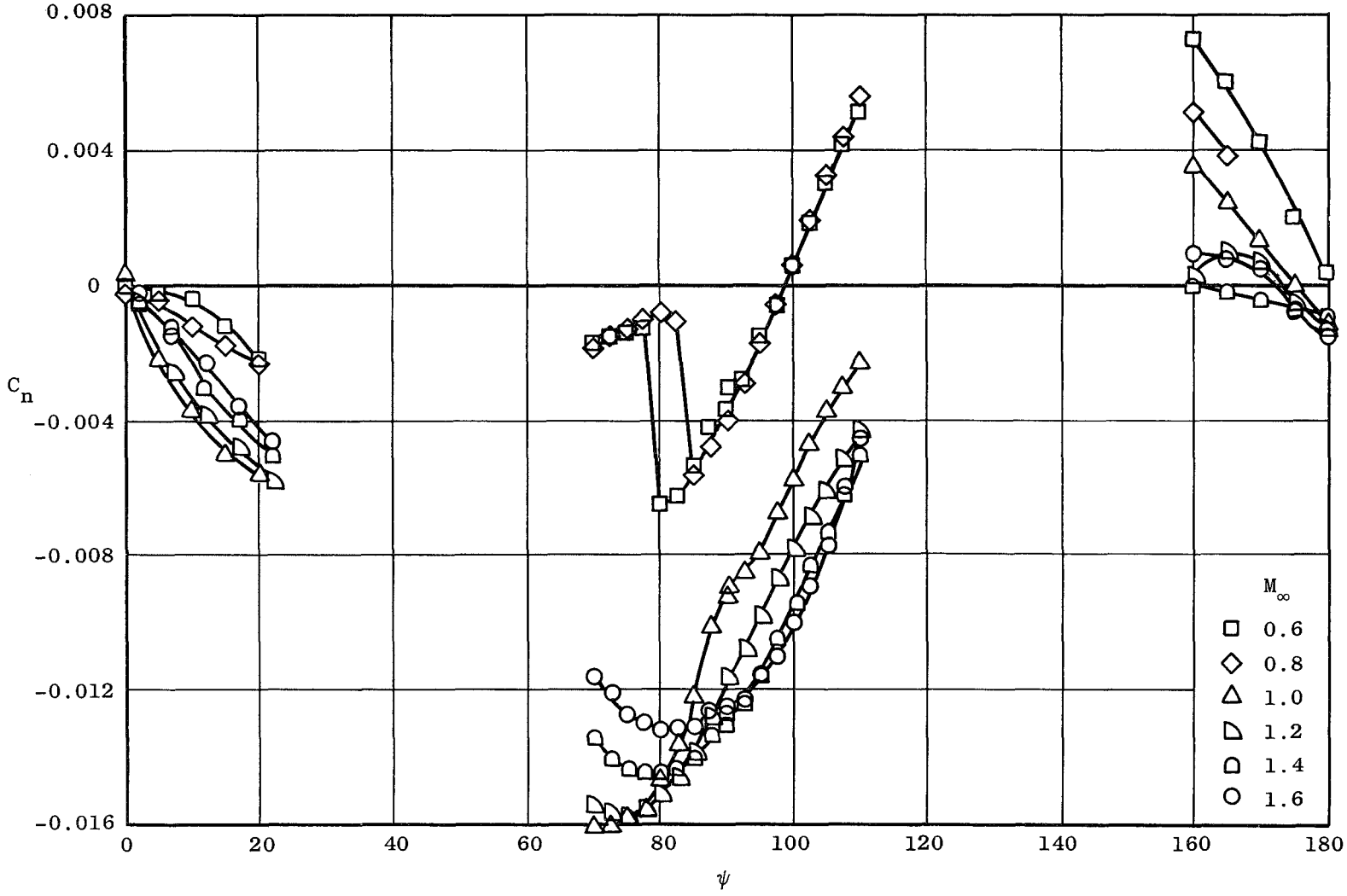

Fig. 21 Variation of Yawing-Moment Coefficient with Yaw Angle, $\alpha = 0$

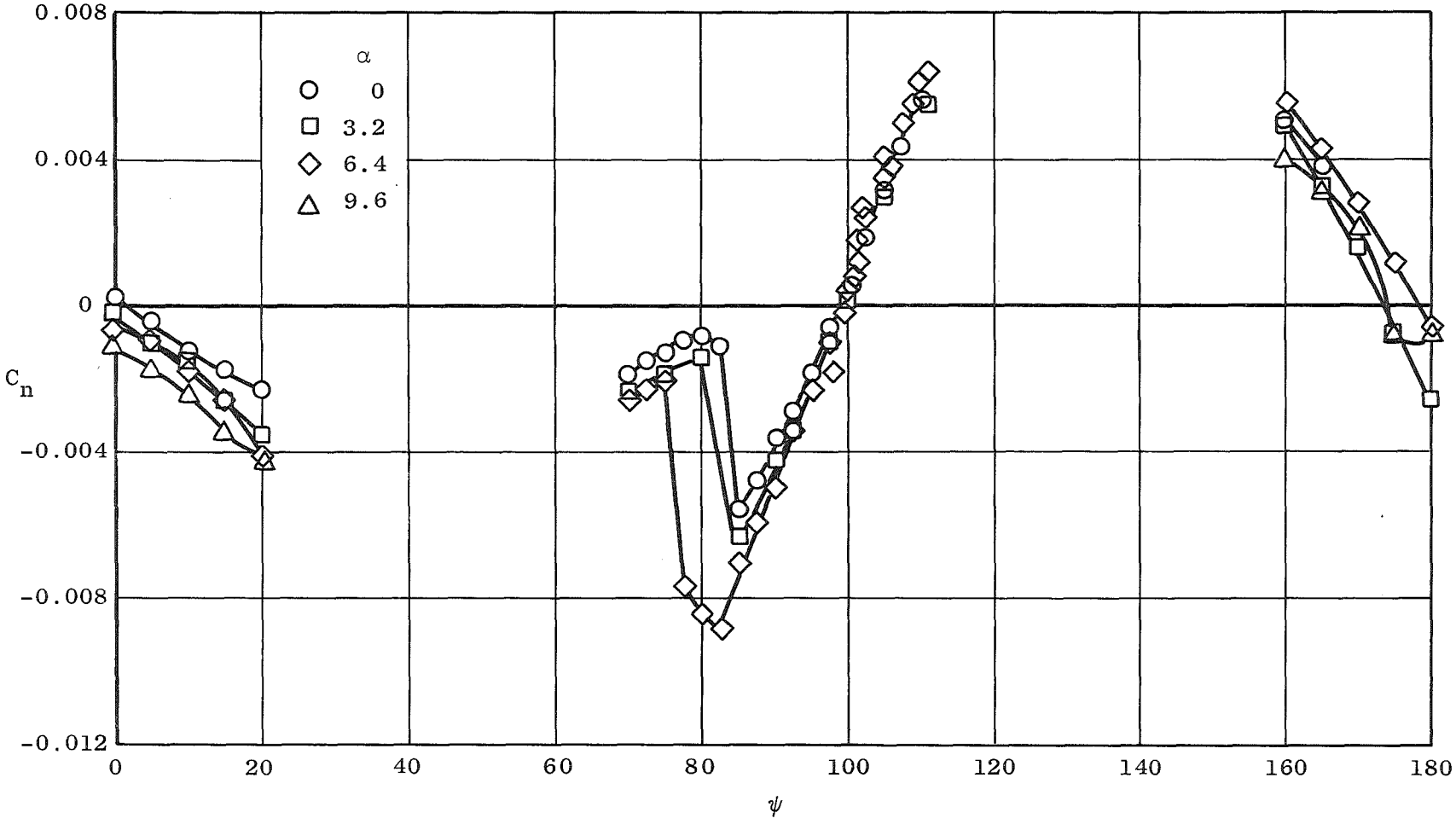

Fig. 22 Variation of Yawing-Moment Coefficient with Yaw Angle, $M_\infty = 0.8$

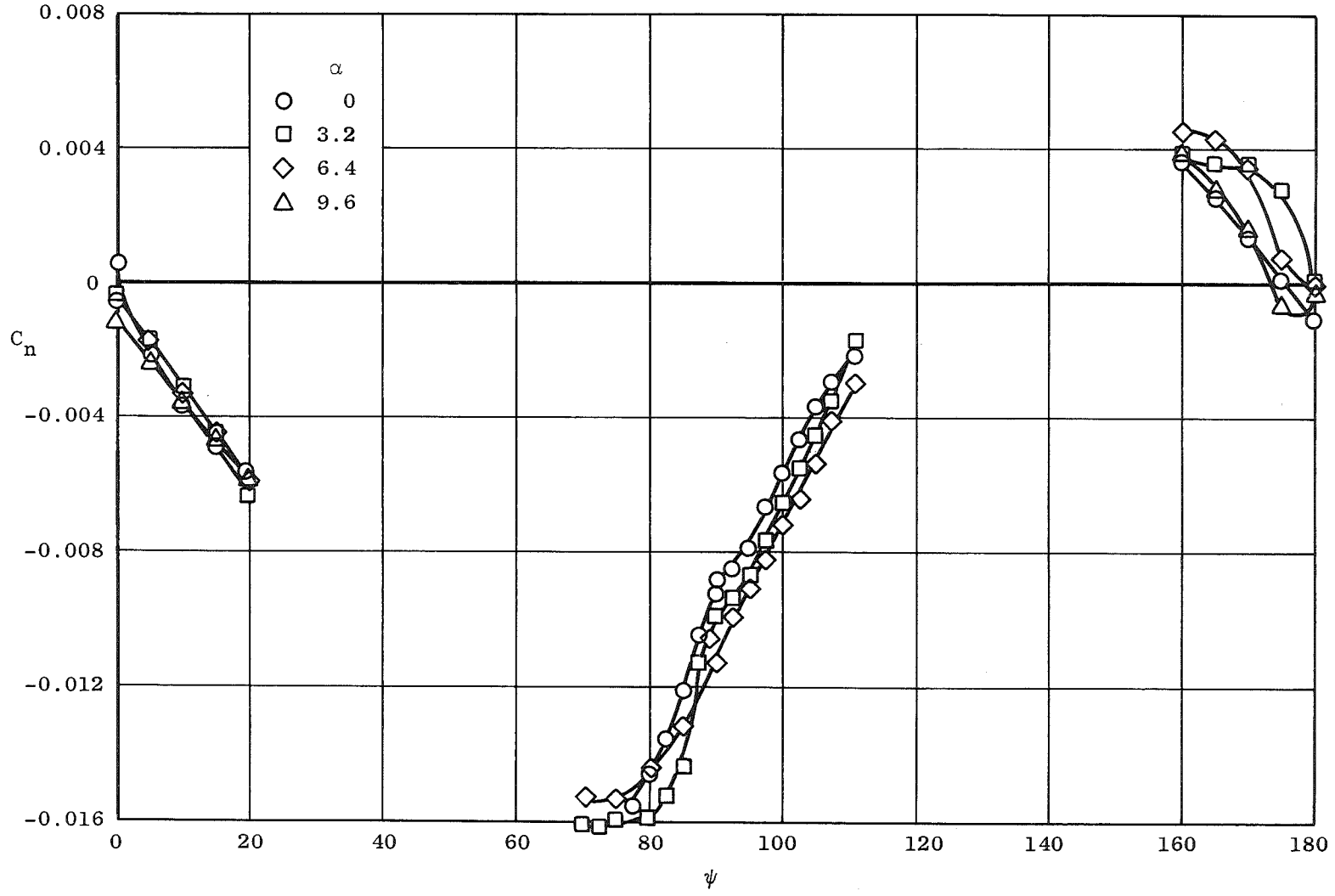

Fig. 23 Variation of Yawing-Moment Coefficient with Yaw Angle, $M_\infty = 1.0$

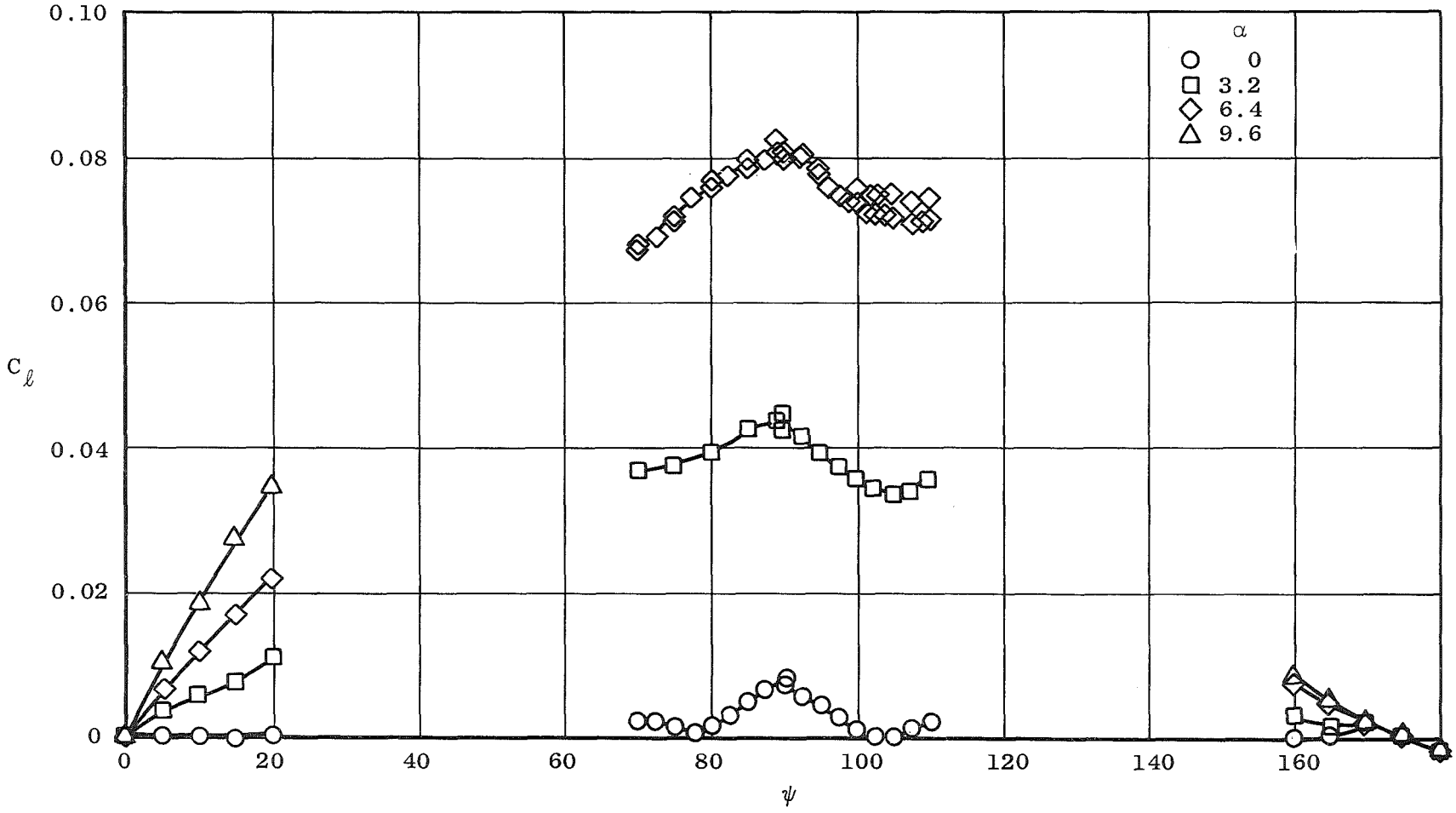

Fig. 24 Variation of Rolling-Moment Coefficient with Yaw Angle, $M_\infty = 0.8$

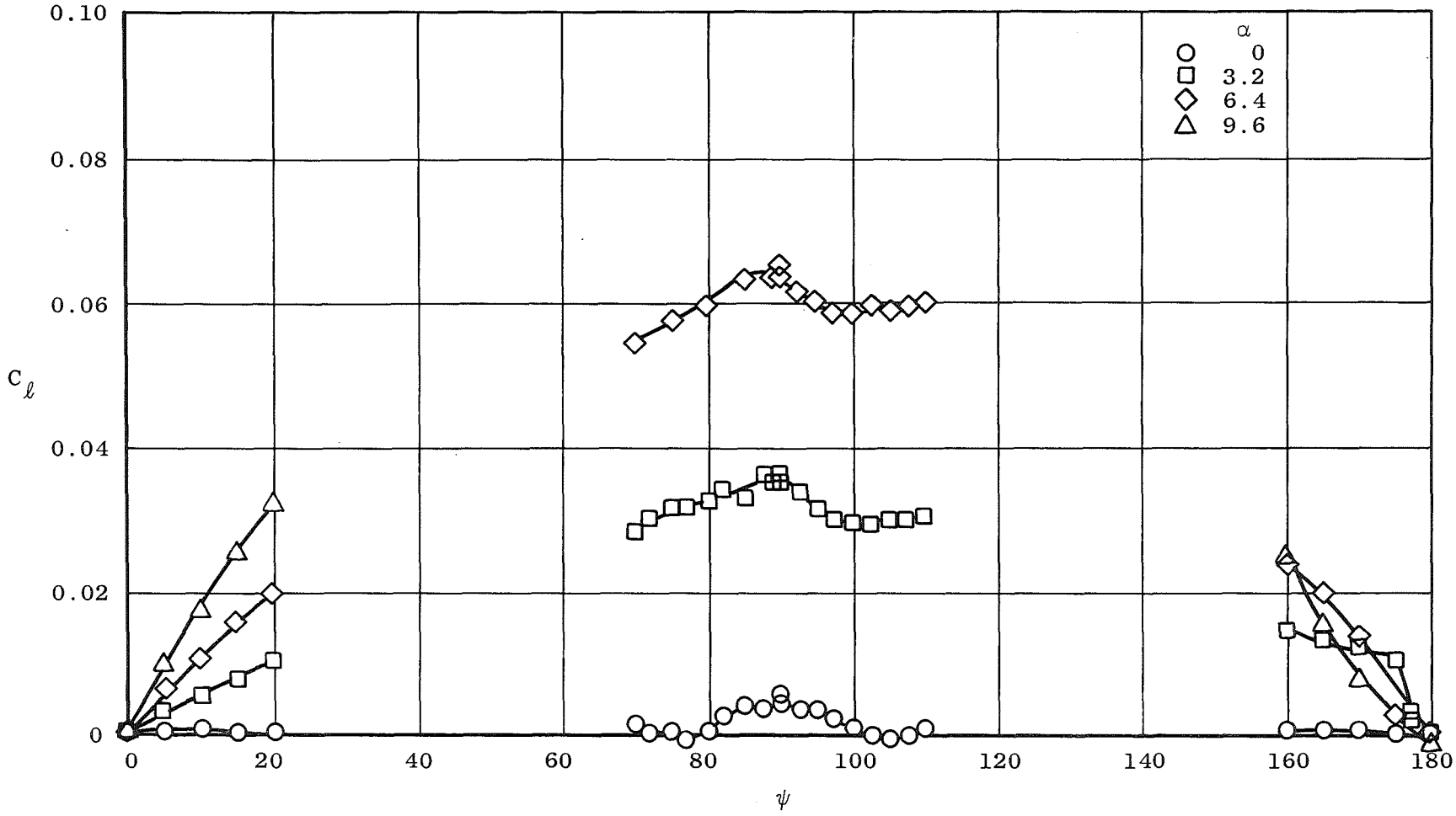

Fig. 25 Variation of Rolling-Moment Coefficient with Yaw Angle, $M_\infty = 1.0$

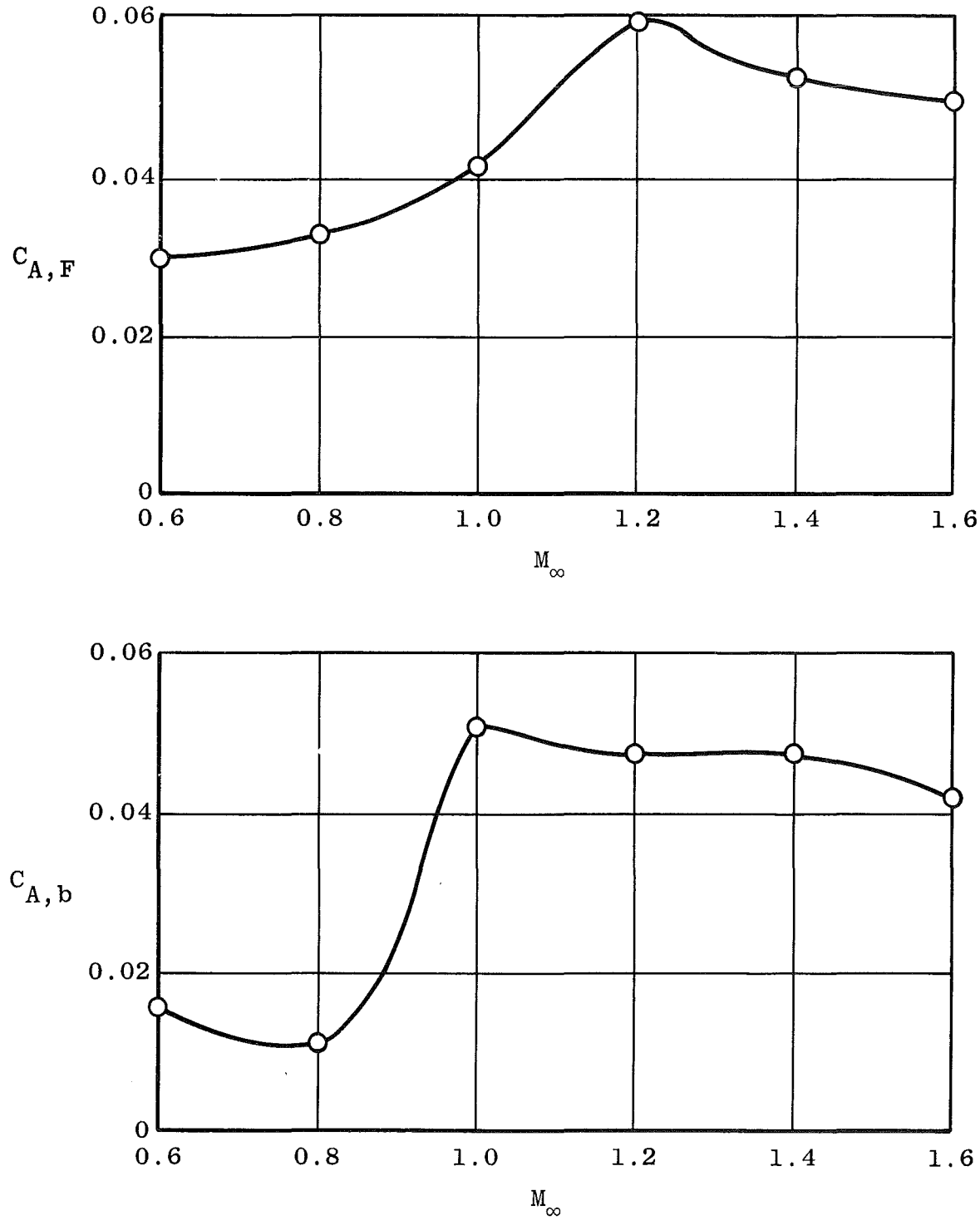

Fig. 26 Variation of Forebody and Base-Drag Coefficient with Mach Number, $\alpha = 0$, $\psi = 0$

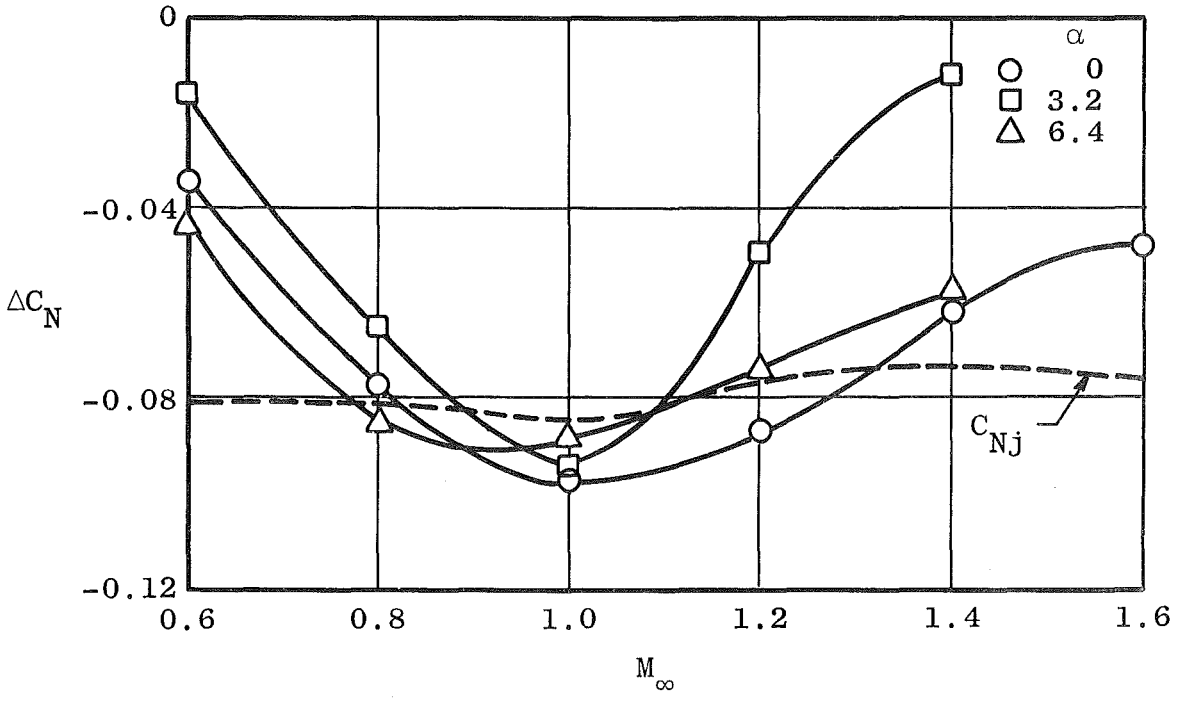

a. Upper Surface Jets-On

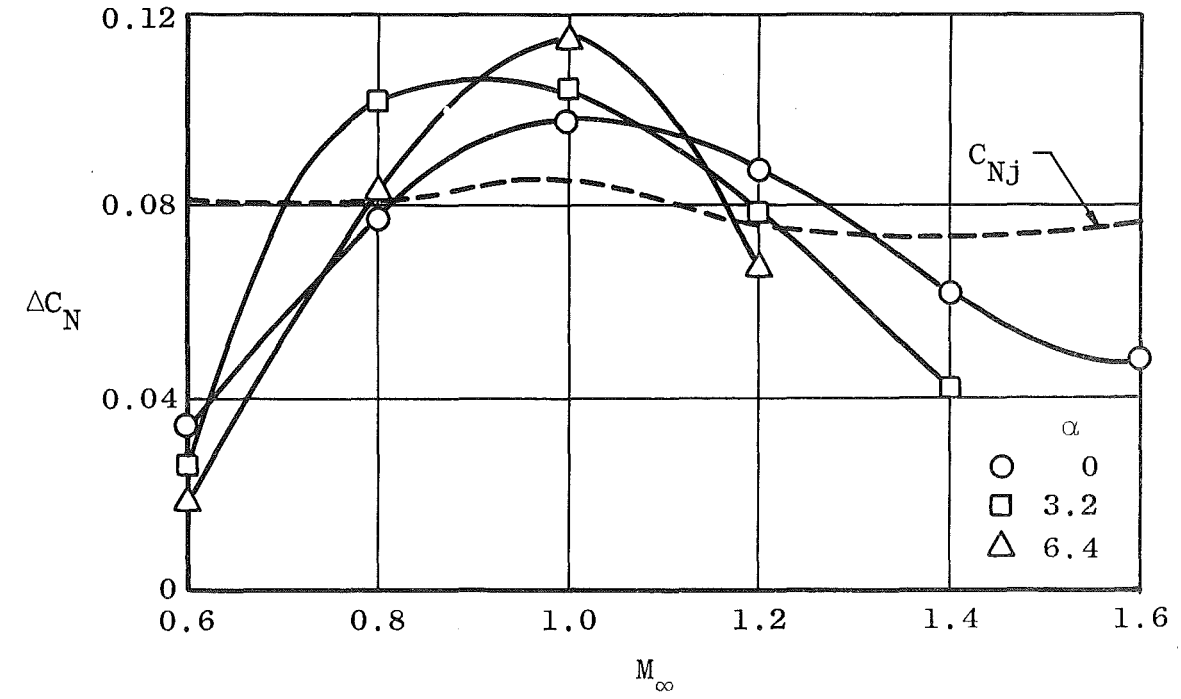

b. Lower Surface Jets-On

Fig. 27 Effect of Jet Flow on Normal-Force Coefficient, $\psi = 0$

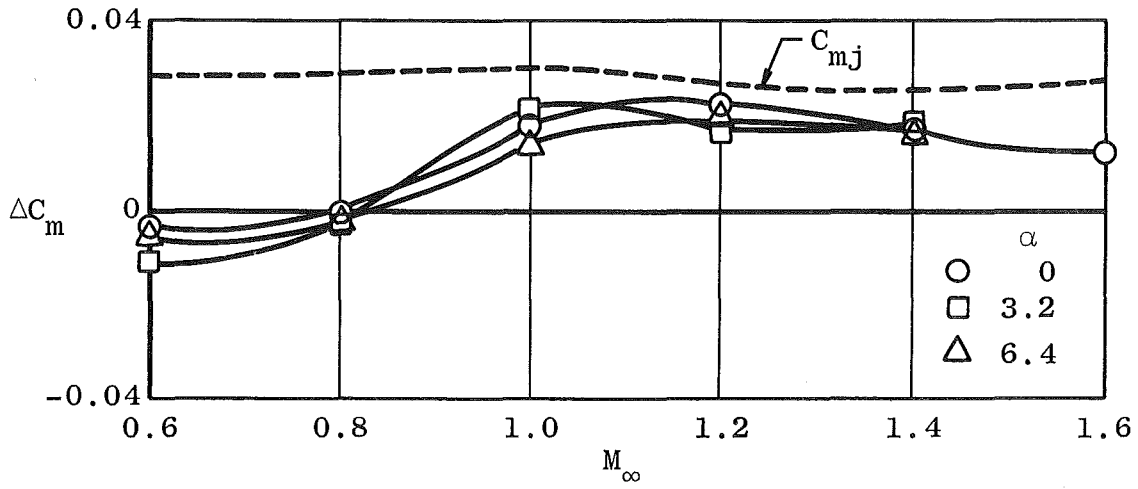

a. Upper Surface Jets-On

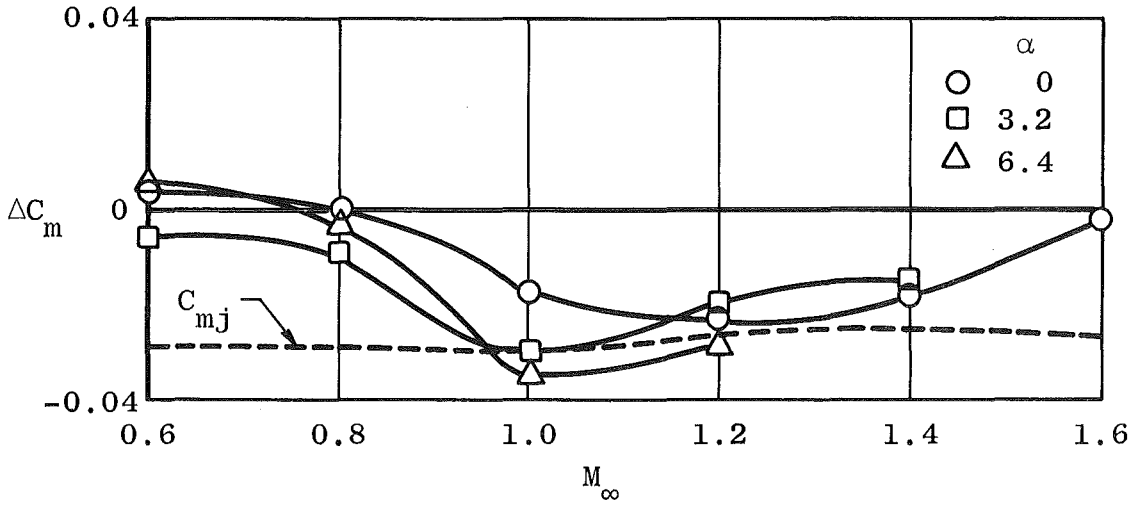

b. Lower Surface Jets-On

Fig. 28 Effect of Jet Flow on Pitching-Moment Coefficient, $\psi = 0$

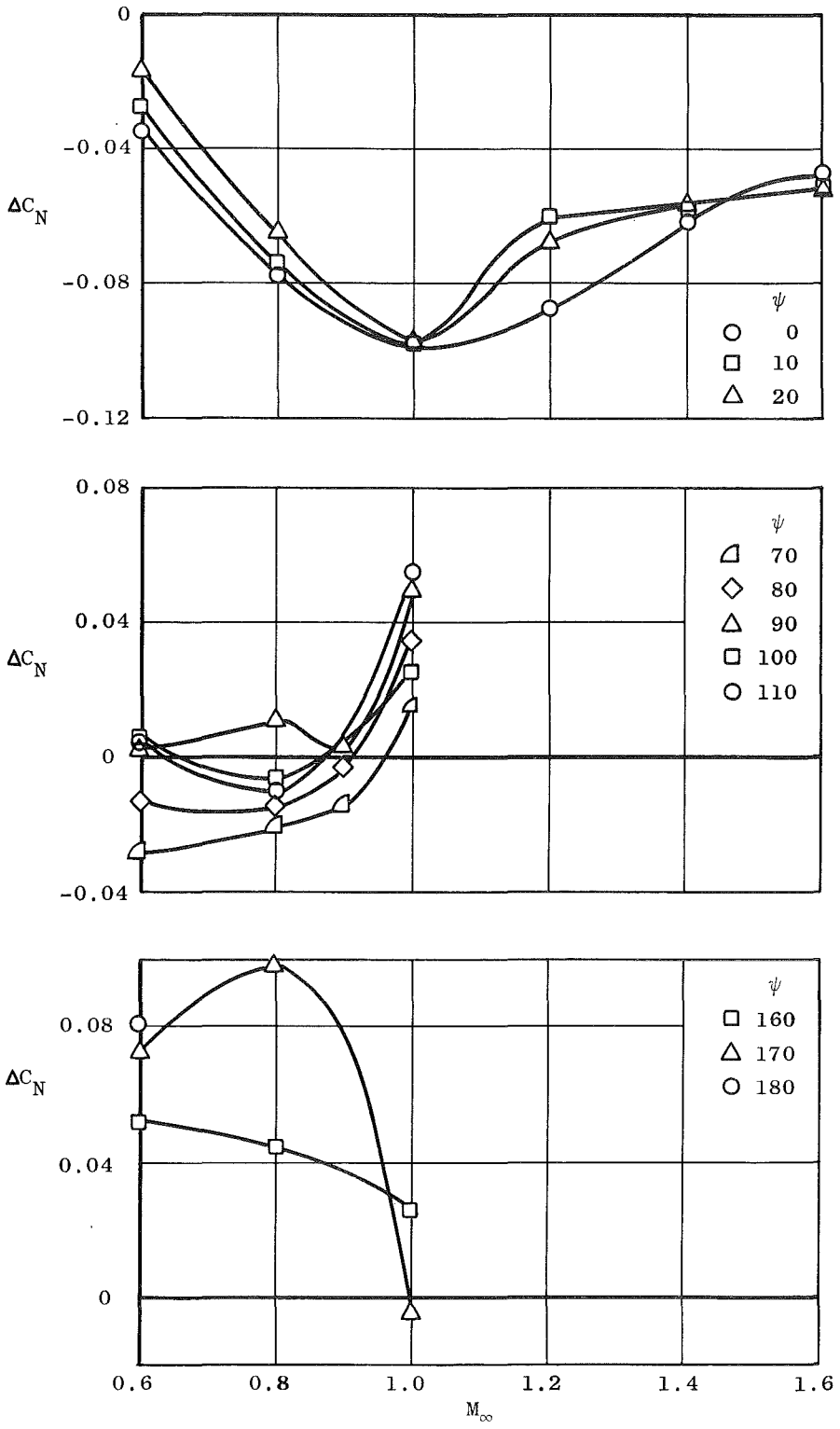

Fig. 29 Effect of Upper Surface Jet Flow on Normal-Force Coefficient, $\alpha = 0$

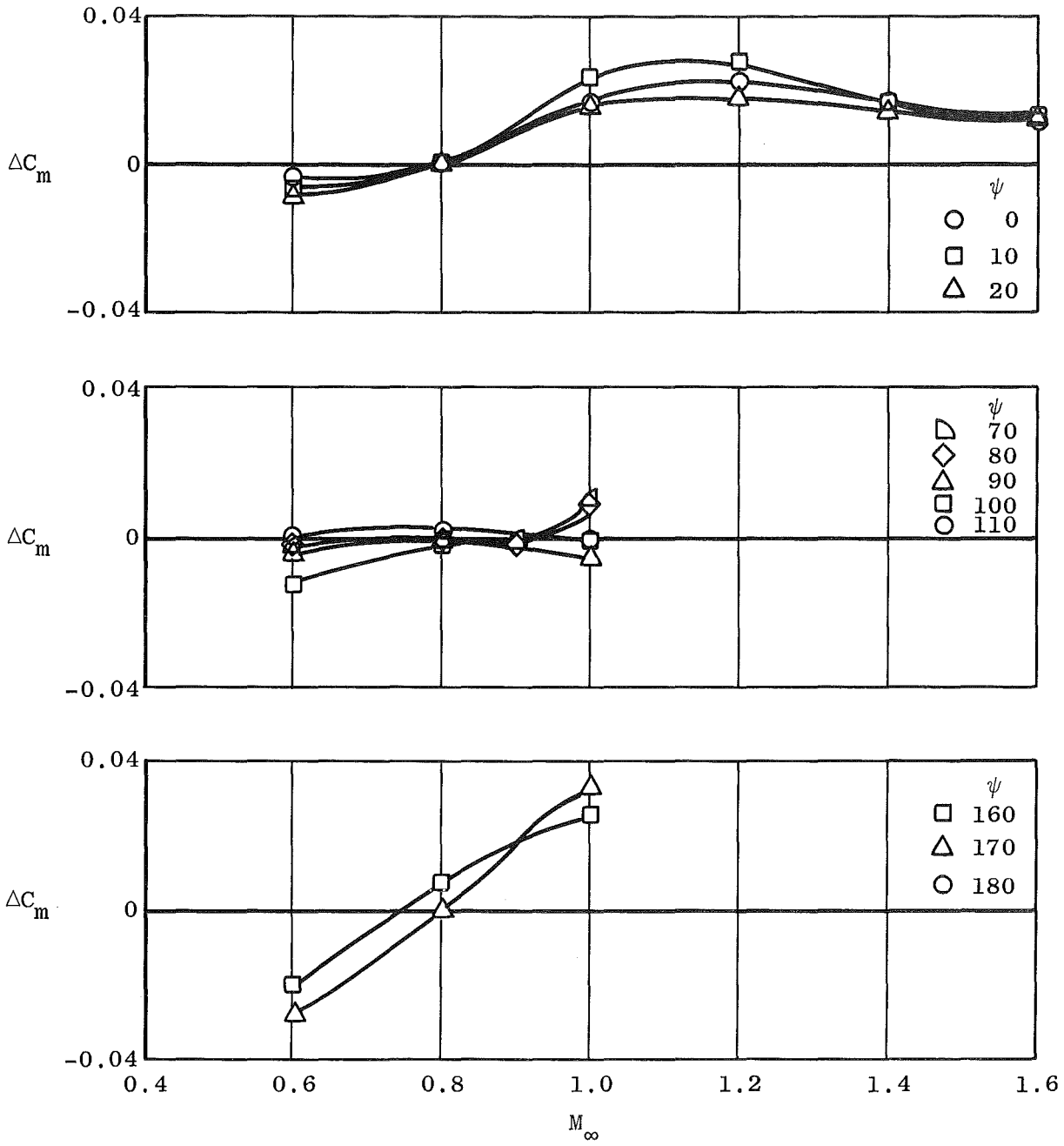

Fig. 30 Effect of Upper Surface Jet Flow on Pitching-Moment Coefficient, $\alpha = 0$

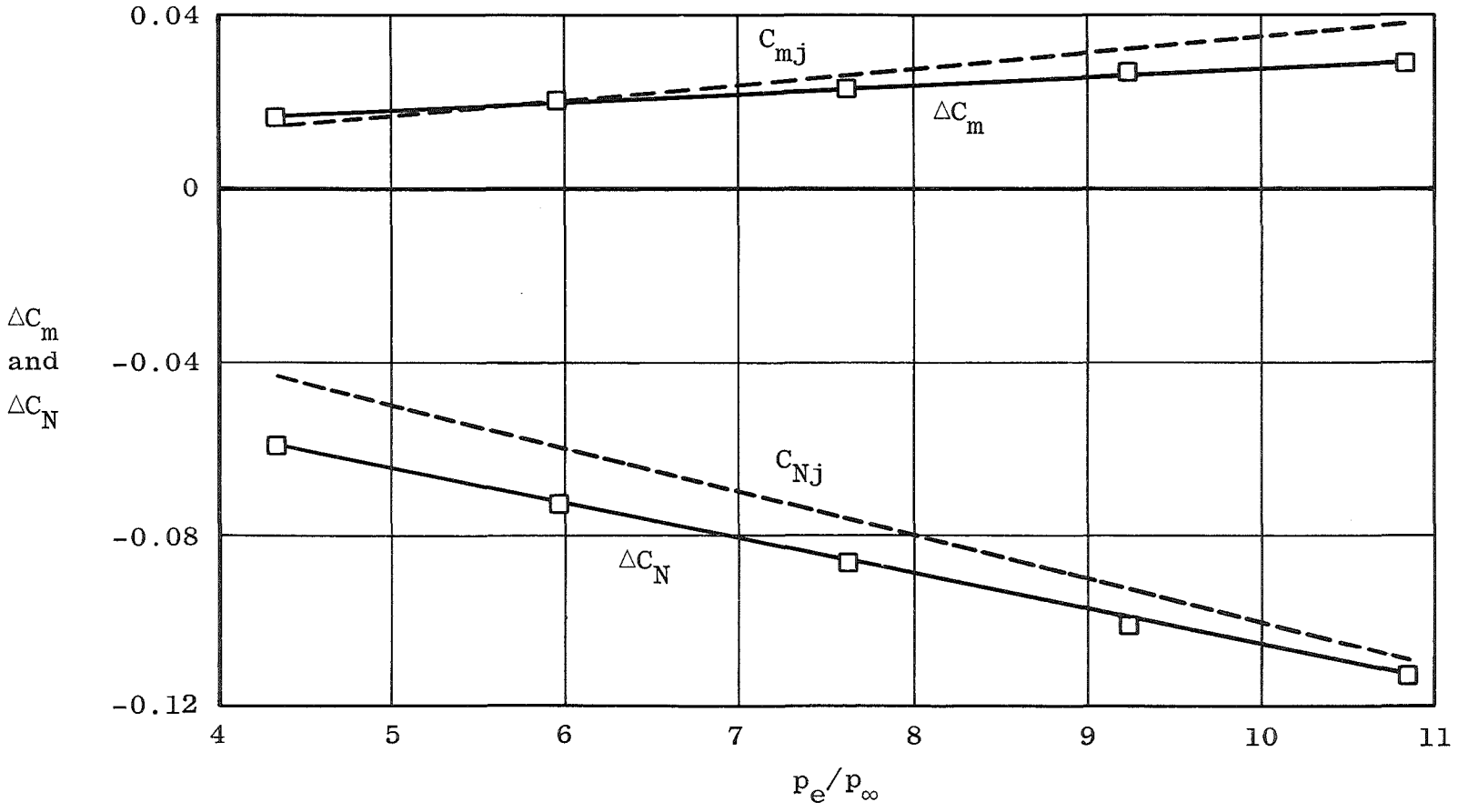

Fig. 31 Effect of Jet Exit Pressure Ratio on Normal-Force and Pitching-Moment Coefficient with Upper Surface Jets On, $M_\infty = 1.2$, $\alpha = 0$, $\psi = 0$

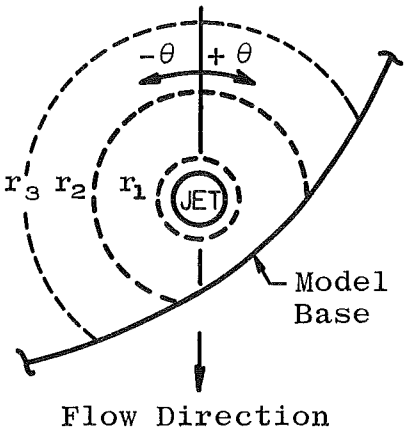

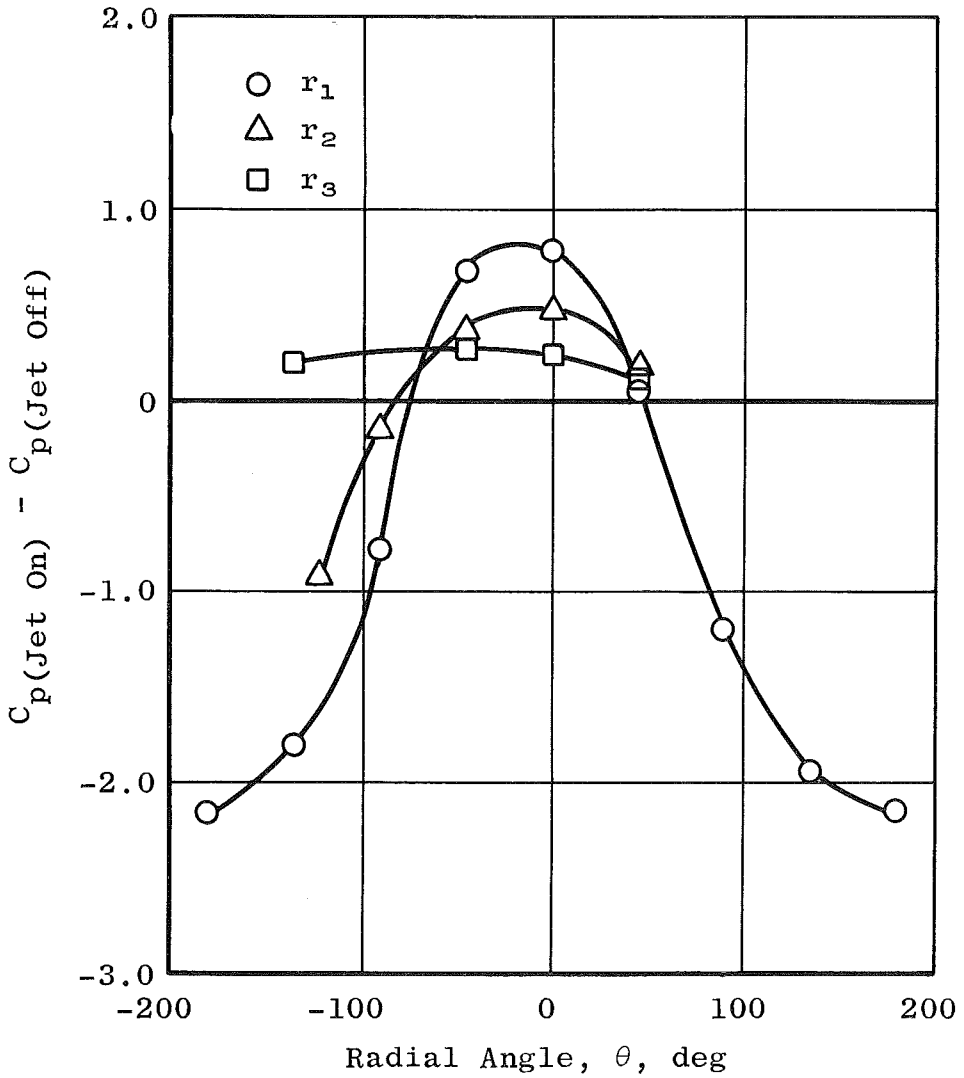

Fig. 32 Influence of Control Jet Flow on Pressure Coefficient Distribution about the Jet Exit, $M_\infty = 0.6$, $\alpha = 0$, $\psi = 0$

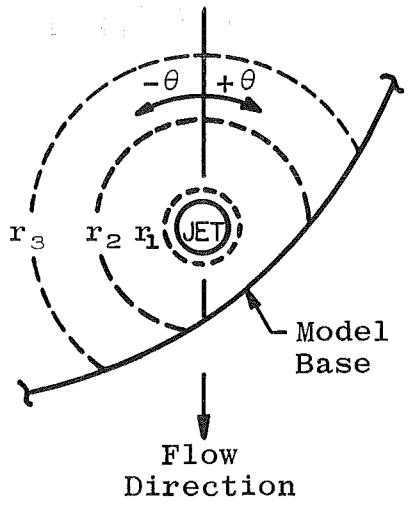

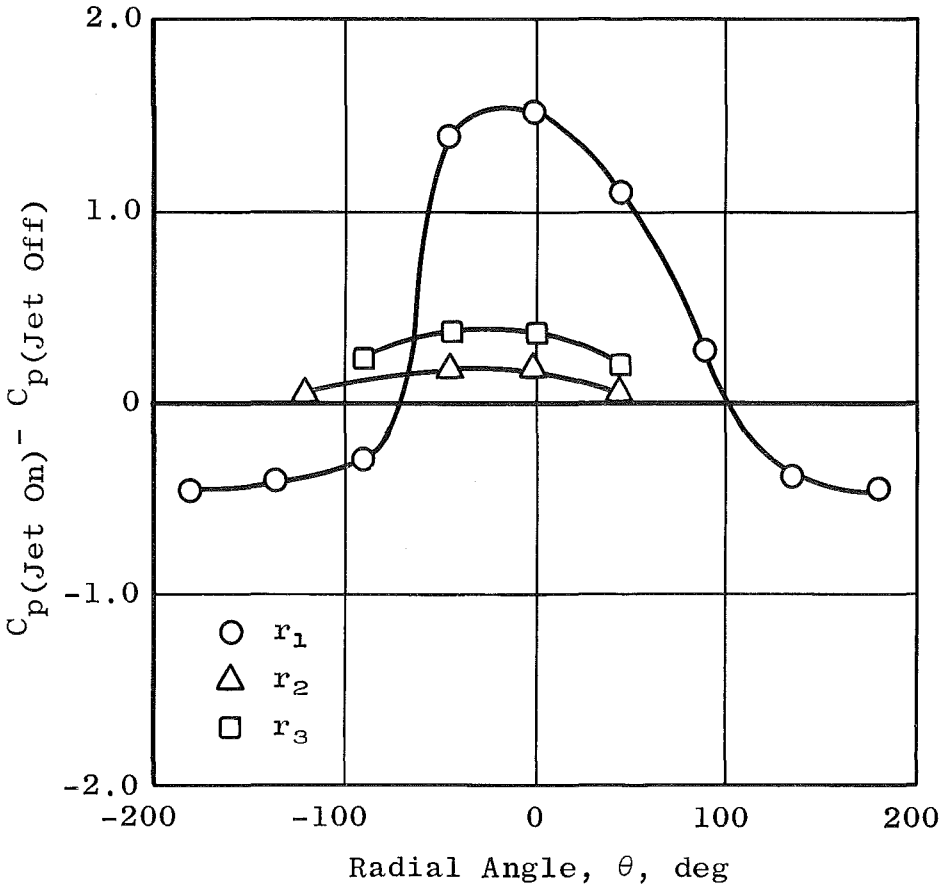

Fig. 33 Influence of Control Jet Flow on Pressure Coefficient Distribution about the Jet Exit, $M_\infty = 1.4$, $\alpha = 0$, $\psi = 0$